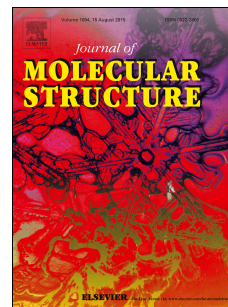


# Accepted Manuscript

*In silico*, *In Vitro* and docking applications for some novel complexes derived from new quinoline derivatives

Ibrahim A.I. Ali, Sahar S.A. El-Sakka, Mohamed H.A. Soliman, Omayma E.A. Mohamed



PII: S0022-2860(19)30777-X

DOI: <https://doi.org/10.1016/j.molstruc.2019.06.053>

Reference: MOLSTR 26695

To appear in: *Journal of Molecular Structure*

Received Date: 4 February 2019

Revised Date: 10 June 2019

Accepted Date: 13 June 2019

Please cite this article as: I.A.I. Ali, S.S.A. El-Sakka, M.H.A. Soliman, O.E.A. Mohamed, *In silico*, *In Vitro* and docking applications for some novel complexes derived from new quinoline derivatives, *Journal of Molecular Structure* (2019), doi: <https://doi.org/10.1016/j.molstruc.2019.06.053>.

This is a PDF file of an unedited manuscript that has been accepted for publication. As a service to our customers we are providing this early version of the manuscript. The manuscript will undergo copyediting, typesetting, and review of the resulting proof before it is published in its final form. Please note that during the production process errors may be discovered which could affect the content, and all legal disclaimers that apply to the journal pertain.

# ***In Silico, In Vitro* and Docking applications for some Novel Complexes Derived from new Quinoline Derivatives**

Ibrahim A. I. Ali<sup>1</sup>, Sahar S. A El-Sakka<sup>2\*</sup>, Mohamed H. A. Soliman<sup>2</sup> and Omayma E. A. Mohamed<sup>3</sup>

<sup>1</sup> Suez Canal University, Faculty of Science, Chemistry Department, Ismailia, Egypt

<sup>2</sup> Suez University, Faculty of Science, Chemistry Department, Suez, Egypt

<sup>3</sup> Chemistry Administrations, Suez, Egypt

\*Corresponding author

Email address: [saharelsakka@hotmail.com](mailto:saharelsakka@hotmail.com); [sahar.alsakka@suezuniv.edu.eg](mailto:sahar.alsakka@suezuniv.edu.eg)

## **Abstract**

The new quinoline derivatives: 2-oxo-1,2-dihydroquinoline-4-carbohydrazide (1), 2-(allyloxy)quinoline-4-carbohydrazide (2), 1-allyl-2-oxo-1,2-dihydroquinoline-4-carbohydrazide (3) and 2-(allylthio)quinoline-4-carbohydrazide (4) and their Cu(II), Ni(II) and Co(II) complexes were synthesized and characterized by using elemental analysis (CHNM%), FTIR, UV/Vis, <sup>1</sup>H NMR, <sup>13</sup>C NMR spectra, DTA, TGA, magnetic susceptibility and the conductivity of 0.001 M in DMSO. The obtained results revealed the formation of the Cu(II) complexes in the square planar form, meanwhile Ni(II) and Co(II) complexes as octahedral structure. The FTIR spectra of the synthesized ligands and their complexes were giving the characteristic stretching vibration bands. The weight loss which appeared in the TG analysis indicates that there are different types of water molecules in the formed complexes. The theoretical calculations which are carried out using different computer programs permit proposing an optimized geometry for the formed complexes. The molecular modeling for the free ligands and their complexes were evaluated and discussed. The energy of the HOMO and LUMO was calculated and discussed. The most stable structure of the synthesized compounds was suggested and its energy was evaluated. The most benefit properties, which play a very important role in drug synthesis with reference to the surface properties of the compounds, were evaluated and discussed. The application of the DFT on the target compounds, gave dipole value around 1.73 D. This result turns out well with the requirement properties of the new drug. Docking the synthesized compounds with HepG2-code: 5EQG protein; e.g. liver carcinoma cell, gave a promising inhibition *in Silico* level. The antimicrobial activity of the target compounds with *E. Coli*, *B. Subtilis* and *Asp. Niger*, *in Vitro* level, gave promising result. The interaction of the compounds with the microorganisms was tested *in Silico* level. *E. Coli* was used as an example for the target microorganism. The protein used for docking process was 5C9T.

**Keywords:** Antimicrobial; Docking; Complexes; In Silico; Quinoline; Hydrazone.

## 1. Introduction

The synthesis of quinoline and its derivatives have attracted considerable attention of organic and medicinal chemists for many years [1]. The structural core of quinoline is frequently associated with medicinal applications [2–5]. The intensive efforts to find effective therapeutic agents with antiviral and antitumor activities have directed many researchers to synthesize a series of quinoline derivatives or their analogues.

The prevalence of the quinoline ring system in a vast range of medical and industrial setting scan is ascribed mainly to its versatility and broad potential for functionalization. In fact, this versatility which earned it the designation of “privileged scaffold” in medicinal chemistry, a term coined by Evans in 1988 which refers to simple structural subunits present in diverse therapeutic compounds with distinctive receptor affinities [6]. Consequently, the synthesis of variously substituted quinolines has been a recurring endeavor for nearly a century and a half [7]. A multitude of synthetic methods has been established over this timeframe, which constructs the quinoline ring from diverse starting materials and result in products with nearly limitless combinations of functionality.

Quinoline and its analogs represent privileged moieties in the field of synthetic and medicinal chemistry because of its diverse chemical and pharmacological properties. The broad spectrum of biological and biochemical activities has been further facilitated by the synthetic versatility of quinoline, which allows the generation of a large number of structurally diverse derivatives [8].

Compounds containing the quinoline ring system were found to be the oldest chemicals for the treatment of various diseases [8]. The extremely drug resistant tuberculosis is a worldwide public health problem in recent years. The wide spread of this disease is primarily due to the development of resistance to the existing drugs that has concerned researchers throughout the world. There is an urgent requirement of improvement in new drug molecules with newer targets and with an alternative mechanism of action [9,10].

It is evident from the literature that quinoline-based hydrazone scaffolds are known to exhibit excellent anti-TB properties [11,12]. This broad spectrum of biological and biochemical activities has been further aided by the synthetic flexibility of quinoline hydrazones, which allows the generation of a large number of structurally diverse derivatives and their metal complexes [13]. Further, various types of hydrazones have attracted continued interest in the medicinal field due to their broad-spectrum biological activities [14]. Among the ligand systems, quinoline hydrazone derivatives are highly important because, these ligands developed due to their diverse chelating ability, structural

flexibility and pharmacological activities like antitumoral, antifungal, antibacterial, antituberculosis, antimalarial, and antiviral [10].

Recently, it is reported that quinoline hydrazones and their Zn(II) complexes showed significant activity against the *Mycobacterium tuberculosis* strain, at low micro-molar levels [15–17].

Recent years have witnessed an unprecedented progress in biological applications of metal coordination compounds of biologically active ligands because of their key role in clinical therapy. Transition metals are particularly suitable for this purpose because they can adopt a wide variety of coordination numbers, geometries and oxidation states in comparison with other main group elements. One of the characteristics of metals is their potential to undergo redox processes, as determined by their redox potentials. Transition metal ions, in particular, are usually able to switch between several oxidation states. Due to the redox activity of metals and, therefore, a possible disturbance of the sensitive cellular redox homeostasis, a tight regulation of the metal and redox balance is crucial for health [18].

On the other hand, over production of activated oxygen species, generated by normal metabolic process, is considered to be the main contributor to oxidative damages to biomolecules such as DNA, lipids and proteins, thus accelerating cancer, aging, inflammation, cardiovascular and neurodegenerative diseases. The potential value of antioxidants has already prompted investigators to search for the cooperative effects of metal complexes and natural compounds for improving antioxidant activity [18].

Depending on their structure, on the one hand, and the source of the oxidative stress, on the other, metal complexes might act as antioxidants or prooxidants. The current review provides insight into the interaction between the reactive oxygen species and the transition metals and their complexes. It will focus on a novel approach to design synthetic antioxidant metal-based compounds and to study their activities in the oxidation processes. This work underlines some important features for the research on metal complexes of biologically active ligands and supports future evaluation of some of these compounds as possible therapeutic agents [18].

Efthimiadou *et.al.*, have prepared and characterized nine metal complexes of the quinolone antibacterial agent N-propyl-norfloxacin with  $\text{VO}^{2+}$ ,  $\text{Mn}^{2+}$ ,  $\text{Fe}^{3+}$ ,  $\text{Co}^{2+}$ ,  $\text{Ni}^{2+}$ ,  $\text{Zn}^{2+}$ ,  $\text{MoO}_2^{2+}$ ,  $\text{Cd}^{2+}$  and  $\text{UO}_2^{2+}$ . The antimicrobial activity of the complexes has been tested on three different microorganisms [19]. The interaction of the complexes with calf-thymus (CT) DNA has also been studied.

According to the history of the important applications of the quinoline derivatives and their metal complexes, this work introduce some new quinoline derivatives and their  $\text{Cu}^{2+}$ ,  $\text{Ni}^{2+}$  and  $\text{Co}^{2+}$  complexes. The new view of the synthesized compounds in the level of *in Vitro* and *in Silico* was

attained to a deep prospective view which facilitates determining which one could be used as drug and which could be toxic.

## 2. Materials and Methods

### 2.1. Materials

All chemicals used in this study were of analytical grade. The primitive chemicals (Koch-Light and Sigma-Aldrich) were used as received. The metals nitrate salts (Cu(II), Ni(II), Co(II)) were purchased from the Sigma-Aldrich and used without extra treatment.

### 2.2. Apparatus

Thin layer chromatography (TLC) was carried out on silica gel type 60-F<sub>254</sub> aluminum sheets (E. Merck, layer thickness= 0.2 mm) using the following solvent systems, S<sub>1</sub>: petroleum ether/ethyl acetate (5:1); S<sub>2</sub>: petroleum ether/ethyl acetate (2:1); S<sub>3</sub>: petroleum ether/ethyl acetate (1:1).

The obtained spots were detected by UV lamp. Melting points were determined on 300 °C melting point apparatus and the values are used without extra correction. The infrared spectra were obtained in the 4000–400 cm<sup>-1</sup> region by using Bruker Alpha instrument with KBr discs. <sup>1</sup>H and <sup>13</sup>C NMR spectra were recorded on Bruker spectrometer operating at 300 and 75.0 MHz uses CDCl<sub>3</sub> as solvent and TMS as internal standard. Elemental analysis was carried out by element arvario instrument. The electronic absorption spectra were obtained on UV-1601PC Shimadzu spectrophotometer in 1 cm quartz cell. TGA and DTA were recorded on Shimadzu 60 thermal analyzer under a dynamic flow of nitrogen (30 mL/min) and heating rate 10 °C/min with open platinum sample holder. Electrical conductivity measurements were carried out at room temperature on freshly prepared 1 mM DMSO solution using WTW conductivity.

### 2.3. Antimicrobial Activity

The antimicrobial activities of the synthesized compounds have been screened using different strains of bacteria (*Bacillus subtilis* and *Escherichia coli*) and pathogenic fungi (*Aspergillus fumigatus*).

The disc diffusion method technique was adopted for antibacterial activity [20] while the well technique was used for antifungal activity [21].

Mean zone of the inhibition in mm ± standard deviation beyond well diameter (6 mm) produced on a range of environmental and clinically pathogenic microorganisms using (30 mg/L) concentration of the tested samples. The test was done using the diffusion agar technique, well diameter: 6.0 mm (30 µL was tested). Ampicillin and Fluconazole were used as positive control while methanol was used as negative control. This test was performed in the Center of Mycology and Biotechnology–Suez Canal University

## 2.4. Synthesis of the Target Complexes

The target complexes were prepared according to the following procedure. The targeted compounds (ligands) (1.0 mmol) were dissolved in 20 mL ethanol. The metal nitrate (0.5 mmol) was dissolved in 10 mL ethanol, which was added dropwise with stirring to the ligand solution. The obtained mixture was refluxed with stirring for 5 h. The formed precipitate was filtered, washed with hot ethanol and dried under vacuum over anhydrous  $\text{CaCl}_2$ .

## 2.5. Synthesis of the Target Quinoline derivatives

### General Methods

Hydrazine hydrate was added to a solution of esters in ethanol or methanol. The reaction mixture was refluxed at 85 °C for 6 hr. After cooling to room temperature the precipitated hydrazides were filtered off, washed with water and ethanol followed by recrystallization from aqueous ethanol or methanol to yield the quinolone derivatives (**Scheme 1**).

### 2.5.1. 2-oxo-1,2-dihydroquinoline-4-carbohydrazide (1)

Faintly beige powder (1.59 g, 88.3%), mp > 300 °C,  $R_f = 0.90$  ( $S_2$ ),  $^1\text{H NMR}$  (300.0 MHz,  $\text{CDCl}_3$ )  $\delta =$  9.96 (2H, br, 2NH), 7.75 (1H, d,  $J = 9.0$  Hz, ArH), 7.54 (1H, t,  $J = 9.0$  Hz, ArH), 7.36 (1H, d,  $J = 6.0$ , ArH), 7.19 (1H, t,  $J = 9.0$  Hz, ArH), 6.48 (1H, s, ArH), 4.55, 3.45 (2H, br,  $\text{NH}_2$ ).  $^{13}\text{C NMR}$  (75.0 MHz,  $\text{CDCl}_3$ )  $\delta =$  165.5 (CO), 161.6 (Ar-CO), 145.5, 139.6, 131.3, 126.4, 122.4, 120.5, 116.8, 116.1 (Ar-C). Anal. Calcd. for  $\text{C}_{10}\text{H}_9\text{N}_3\text{O}_2$  (203.20): C, 59.11; H, 4.46; N, 20.68. Found: C, 59.34; H, 4.18; N, 20.45.

### 2.5.2. 2-(allyloxy)quinoline-4-carohydrazide (2)

White powder (1.2 g, 75.0%), m.p 168 °C,  $R_f = 0.67$  ( $S_2$ ).  $^1\text{H NMR}$  (300.0 MHz,  $\text{CDCl}_3$ )  $\delta =$  9.88 (1H, br, NH), 8.05 (1H, d,  $J = 9.0$  Hz, ArH), 7.80 (1H, d,  $J = 9.0$  Hz, ArH), 7.72-7.67 (1H, m, ArH), 7.48-7.43 (1H, m, ArH), 6.97 (1H, s, ArH), 6.25-6.12 (1H, m, CH=), 5.52, 5.34 (2H, 2d,  $J = 18.0, 12.0$  Hz, = $\text{CH}_2$ ), 5.06 (2H, d,  $\text{CH}_2\text{O}$ ), 4.66 (2H, br,  $\text{NH}_2$ ).  $^{13}\text{C NMR}$  (75.0 MHz,  $\text{CDCl}_3$ )  $\delta =$  165.8 (CO), 161.5 (Ar-CO), 146.8, 144.6 (Ar-C), 133.3 (CH=), 130.5, 127.5, 125.9, 124.9, 122.1 (Ar-C), 117.8 (=CH<sub>2</sub>), 111.7 (Ar-C), 67.7 ( $\text{OCH}_2$ ). Anal. Calcd. for  $\text{C}_{13}\text{H}_{13}\text{N}_3\text{O}_2$  (243.27): C, 64.4; H, 5.39; N, 17.27. Found: C, 64.02; H, 5.69; N, 17.46.

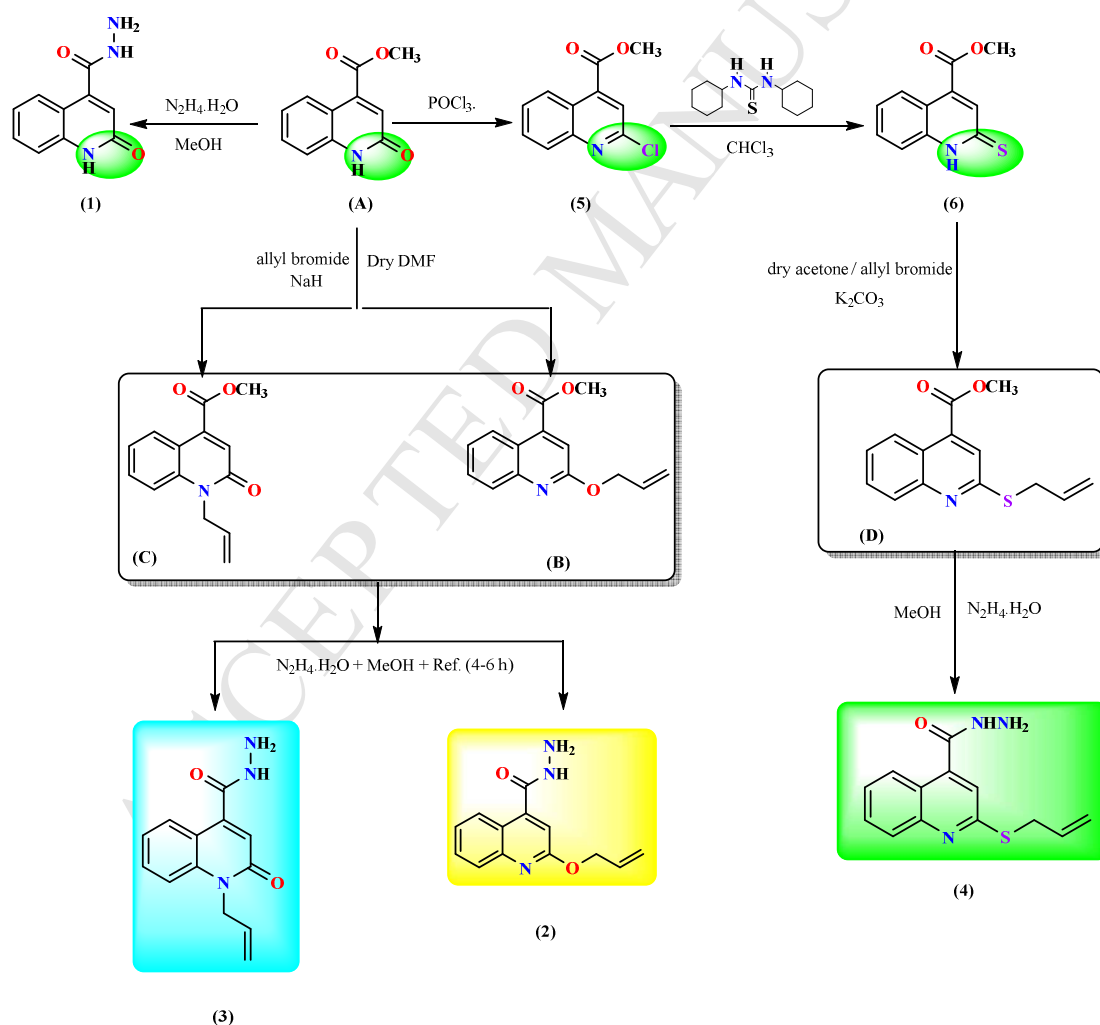
### 2.5.3. 1-allyl-2-oxo-1,2-dihydroquinoline-4-carbohydrazid (3)

Yellow crystals (0.65 g, 54.2%), m.p 267-269 °C,  $R_f = 0.50$  ( $S_3$ ).  $^1\text{H NMR}$  (300.0 MHz,  $\text{CDCl}_3$ )  $\delta =$  9.90 (1H, s, NH), 7.82 (1H, d,  $J = 9.0$  Hz, ArH), 7.63 (1H, t,  $J = 9.0$  Hz, ArH), 7.50 (1H, d,  $J = 9.0$  Hz, ArH), 7.28 (1H, t,  $J = 9.0$  Hz, ArH), 6.61 (1H, s, ArH), 6.00-5.88 (1H, m, CH=), 5.16, 5.00 (2H, 2d,  $J = 12.0, 18.0$  Hz, = $\text{CH}_2$ ), 4.93 (2H, d,  $J = 6.0$  Hz,  $\text{CH}_2\text{N}$ ), 4.63 (2H, s,  $\text{NH}_2$ ).  $^{13}\text{C NMR}$  (75.0 MHz,  $\text{CDCl}_3$ )  $\delta =$  165.4 (CO), 160.6 (Ar-CO), 144.8, 139.5 (Ar-C), 132.8 (CH=), 131.6, 127.2, 122.6, 119.6,

117.9 (Ar-C), 117.0 (=CH<sub>2</sub>), 116.0 (Ar-C), 44.1 (NCH<sub>2</sub>). Anal. Calcd. for C<sub>13</sub>H<sub>13</sub>N<sub>3</sub>O<sub>2</sub> (243.27): C, 64.4; H, 5.39; N, 17.27. Found: C, 64.27; H, 5.55; N, 17.41

#### 2.5.4. 2-(allylthio)quinoline-4-carbohydrazide (4)

Beige powder (1 g, 83.3%), m.p 156-158 °C, R<sub>f</sub> = 0.64, (S<sub>1</sub>). <sup>1</sup>H NMR (300.0 MHz, CDCl<sub>3</sub>) δ= 8.50 (1H, d, NH↔OH), 8.09 (1H, d, J= 6.0 Hz, Ar-H), 7.93 (1H, d, J= 9.0 Hz, ArH), 7.75 (1H, t, J= 6.0 Hz, ArH), 7.54 (1H, t, J= 6 Hz, ArH), 7.35 (1H, s, ArH), 6.10-5.95 (1H, m, CH=), 5.45, 5.15 (2H, 2d, J= 15.0, 9.0 Hz, =CH<sub>2</sub>), 4.30 (2H, br, NH<sub>2</sub>), 4.02 (2H, d, J= 6.0 Hz, SCH<sub>2</sub>). <sup>13</sup>C NMR (75.0 MHz, CDCl<sub>3</sub>) δ= 165.7 (CO), 158.4 (CS), 148.3, 141.3 (Ar-C), 134.2 (CH=), 130.7, 128.3, 126.4, 126.0, 122.9, 14.1 (Ar-C), 118.5 (=CH<sub>2</sub>), 32.3 (SCH<sub>2</sub>). Anal. Calcd. for C<sub>13</sub>H<sub>13</sub>N<sub>3</sub>OS (259.33): C, 60.21; H, 5.05; N, 16.20. Found: C, 60.32; H, 5.17; N, 16.43.



**Scheme 1:** The stepwise formation of the synthesized ligands 1-4.

### 3. Results and Discussion

The obtained complexes which were formed from the reaction of the target ligands (**1-4**) with the M(II) ions (M= Cu, Ni and Co) were purified and characterized by using different tools, which were depicted as follows:

#### 3.1. Elemental Analysis and Physical Properties:

The elemental analysis of the complexes which were formed from the ligand **1** and M(II) ions was listed in **Table 1**. The postulated formula could be represented as follows:  $[\text{Co}(\text{C}_{10}\text{H}_9\text{N}_3\text{O}_2)_2(\text{H}_2\text{O})_2](\text{NO}_3)_2$ ,  $[\text{Ni}(\text{C}_{10}\text{H}_9\text{N}_3\text{O}_2)_2(\text{H}_2\text{O})_2](\text{NO}_3)_2$  and  $[\text{Cu}(\text{C}_{10}\text{H}_9\text{N}_3\text{O}_2)_2](\text{NO}_3)_2 \cdot (\text{H}_2\text{O})_2$ . Co(II) complexes are formed as cream non-hygroscopic crystals, Ni(II) as ice blue crystals and Cu(II) as green crystals.

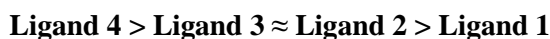
The interaction of the ligand **2** ( $\text{C}_{13}\text{H}_{13}\text{N}_3\text{O}_2$ ) with the Co(II), Ni(II) and Cu(II) ions gave the corresponding complexes which could be formulated as:  $[\text{Co}(\text{C}_{13}\text{H}_{13}\text{N}_3\text{O}_2)_2(\text{H}_2\text{O})_2](\text{NO}_3)_2$ ,  $[\text{Ni}(\text{C}_{13}\text{H}_{13}\text{N}_3\text{O}_2)_2(\text{H}_2\text{O})_2](\text{NO}_3)_2$  and  $[\text{Cu}(\text{C}_{13}\text{H}_{13}\text{N}_3\text{O}_2)_2](\text{NO}_3)_2 \cdot (\text{H}_2\text{O})_4$ , respectively. The obtained elemental analysis (N and M%) goes well with the postulated formula (**Table 1**). All the complexes were crystalline and non-hygroscopic. Co(II) complex has brown fine crystals, Ni(II) complex gave green crystal and Cu(II) complex has green crystals.

The complexes which derived from the ligand **3** and the target metals ions gave elemental analysis as shown in **Table 1**. The obtained results revealed the following postulated formula:  $[\text{Co}(\text{C}_{13}\text{H}_{13}\text{N}_3\text{O}_2)_2(\text{H}_2\text{O})_2](\text{NO}_3)_2$ ,  $[\text{Ni}(\text{C}_{13}\text{H}_{13}\text{N}_3\text{O}_2)_2(\text{H}_2\text{O})_2](\text{NO}_3)_2$  and  $[\text{Cu}(\text{C}_{13}\text{H}_{13}\text{N}_3\text{O}_2)_2](\text{NO}_3)_2 \cdot (\text{H}_2\text{O})_2$ . All the complexes have fine crystal structure and non-hygroscopic behavior. Co(II) complex has orange color, Ni(II) complex was ice blue meanwhile Cu(II) was turquoise.

The interaction of the ligand **4** ( $\text{C}_{13}\text{H}_{13}\text{N}_3\text{OS}$ ) with the Co(II) ions gave brown, non-hygroscopic crystals with the molecular formula:  $[\text{Co}(\text{C}_{13}\text{H}_{13}\text{N}_3\text{OS})_2(\text{H}_2\text{O})_2](\text{NO}_3)_2 \cdot (\text{H}_2\text{O})_4$ . Ni(II) ions gave brown crystals with the formula:  $[\text{Ni}(\text{C}_{13}\text{H}_{13}\text{N}_3\text{OS})_2(\text{H}_2\text{O})_2](\text{NO}_3)_2 \cdot (\text{H}_2\text{O})_2$ . The brown crystals also formed with Cu(II) ions with the formula:  $[\text{Cu}(\text{C}_{13}\text{H}_{13}\text{N}_3\text{OS})_2](\text{NO}_3)_2$  (**Table 1**).

#### 3.2. Conductivity of the Complexes:

The conductivity of the formed complexes was measured in DMSO (0.001 M). All the formed complexes gave conductivity in the range 140-179  $\mu\text{S}$  ( $\text{ohm}^{-1} \cdot \text{cm}^2 \cdot \text{mol}^{-1}$ ), which indicates the electrolytic behavior of the complexes [22], which could be formulated generally as  $[\text{A}](\text{NO}_3)_2$  form (**Table 1**) [23–25]. Generally, the conductivity of the formed complexes has the following order:



Cu(II) complexes gave the lowest conductivity, meanwhile Co(II) and Ni(II) complexes were close to each other. The obtained result is manifested in the following points:

1. Cu(II) complex has a structure different from the other complexes,
2. Co(II) and Ni(II) complexes could have a similar structure.

### 3.3. FTIR Spectra:

The FTIR spectra of the target ligands and their complexes were listed in **Table 2** and shown in **Figures 1–4** as representative examples.

Ligand **2** gave a broad and strong band centered at wavenumber  $3454\text{ cm}^{-1}$  which could be attributed to the stretching vibrational motion for O-H group with some inter and/or intra hydrogen bond [22]. The obtained result strongly indicated the presence of some tautomerism from the type keto $\leftrightarrow$ enol form. The band which appeared at  $3277\text{ cm}^{-1}$  as strong band could be due to  $\nu_{\text{N-H}}$  moiety. The stretching vibrational bands which appeared at  $1640$  and  $1604\text{ cm}^{-1}$  as medium and strong bands, respectively could be attributed to the stretching vibration of the C=O and C=N bonds, respectively [26]. Strong and broad band clearly appeared for all complexes, which ranged at  $3632\text{--}2700\text{ cm}^{-1}$ ,  $3665\text{--}2765\text{ cm}^{-1}$  and  $3651\text{--}2804\text{ cm}^{-1}$  for Cu(II), Ni(II) and Co(II) complexes, respectively, could be assigned as stretching vibration of the water molecules which could be present in the formed complexes as water of coordination and water of crystallization. The broadness could be due to: (1) the presence of strong inter and/ or intra hydrogen bond, (2) the presence of partial overlapping of the wave number of  $\nu_1$  and  $\nu_3$  of the water molecules [27]. The stretching vibration band of C=O were shifted in all formed complexes. This indicates the ligation behavior of this group in complex formation (**Table 2**). The vibration bands of the nitrate group appeared at the wave number range  $1381\text{--}1396\text{ cm}^{-1}$  as strong band, which strongly revealed the ionization nature of this group in the formed complexes [28]. The stretching vibration band of the M-O bond appeared at  $586\text{--}657\text{ cm}^{-1}$  range for all complexes, while M-N appeared at  $514\text{--}520\text{ cm}^{-1}$  as weak band [29]. The stretching vibration value is different from metal to another, where it depends on the electronegativity, electronic structure and the mass of the metal ions [28].

The IR spectrum of the third ligand was listed in **Table 2**. The band which appeared at  $3438\text{ cm}^{-1}$  as shoulder and broad could be due to the presence of the keto $\leftrightarrow$ enol tautomerism with some inter and/ or intra hydrogen bond interaction. The strong band which appeared at  $3347$  and  $3270\text{ cm}^{-1}$  could be assigned as the stretching vibration band due to the NH and NH<sub>2</sub>. The  $\nu_{\text{C=O}}$  appeared at  $1634$  and  $1581\text{ cm}^{-1}$  as strong bands. The band which centered at  $3431\text{ cm}^{-1}$ ,  $3425\text{ cm}^{-1}$  and  $3439\text{ cm}^{-1}$  for Cu(II), Ni(II) and Co(II) complexes, respectively could be due to the stretching vibration of the water molecules which could be present in the formed complexes. The  $\nu_{\text{N-H}}$  of the ligand completely disappeared in Cu (II) complexes or gave red shifted (decreasing in wavenumber) in Ni (II) and Co (II) complexes enhanced the ligation postulation of the nitrogen of the hydrazine moiety in the complexation process. Correspondingly, the variation of the stretching vibration of the C=O, indicates

the entrance of this group in the complexation process. The stretching vibration band, which centered at 1388, 1387 and 1379  $\text{cm}^{-1}$  as strong band for the Cu(II), Ni(II) and Co(II) complexes, respectively, enhanced the ionic behavior of the nitrate group. The M-O and M-N were listed in **Table 2** as weak bands.

The IR spectrum of the ligand **1** gave the characteristic bands for the function groups. The broad and medium band which centered at 3438  $\text{cm}^{-1}$  could be due to the keto $\leftrightarrow$ enol tautomerism. Meanwhile, the NH and  $\text{NH}_2$  appeared at 3270 and 3202  $\text{cm}^{-1}$ . The  $\nu_{\text{C=O}}$  and  $\nu_{\text{C=N}}$  appeared at 1653 and 1517  $\text{cm}^{-1}$ , respectively. The IR spectra of the complexes (**1-Cu**, **1-Ni** and **1-Co**) strongly enhanced the ligation properties of the C=O and  $\text{NH}_2$  groups [22,27,28].

The IR spectra of the ligand **4** and their complexes (**4-Cu**, **4-Ni** and **4-Co**) revealed the close similarity with the ligand **2** and their complexes (**2-Cu**, **2-Ni** and **2-Co**) (**Table 2**).

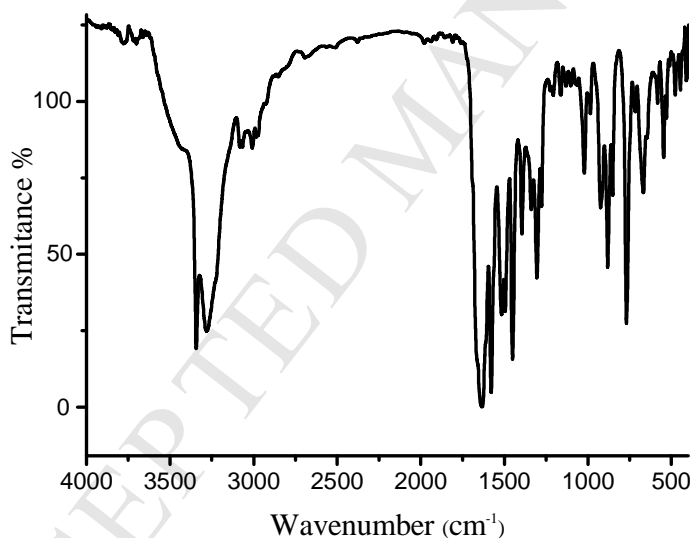


**Figure 1:** FTIR sprum of the ligand **3**.

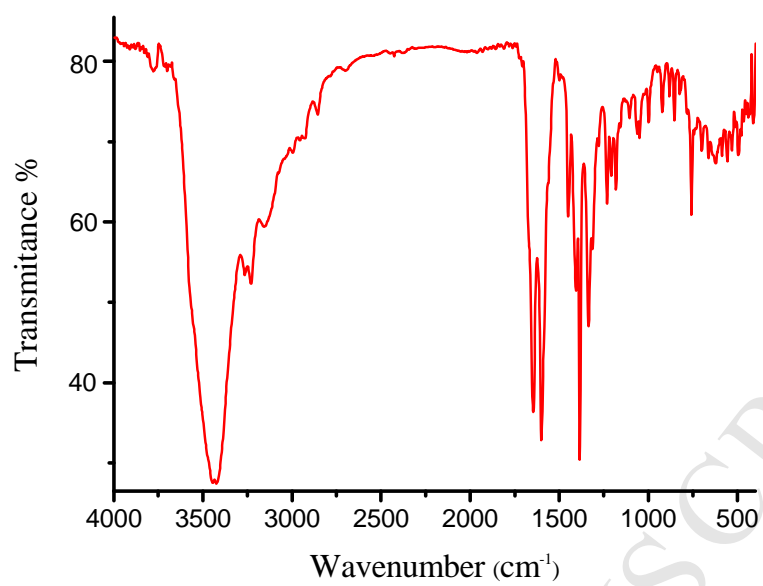


**Figure 2:** FTIR spectrum of compound 3-Co.

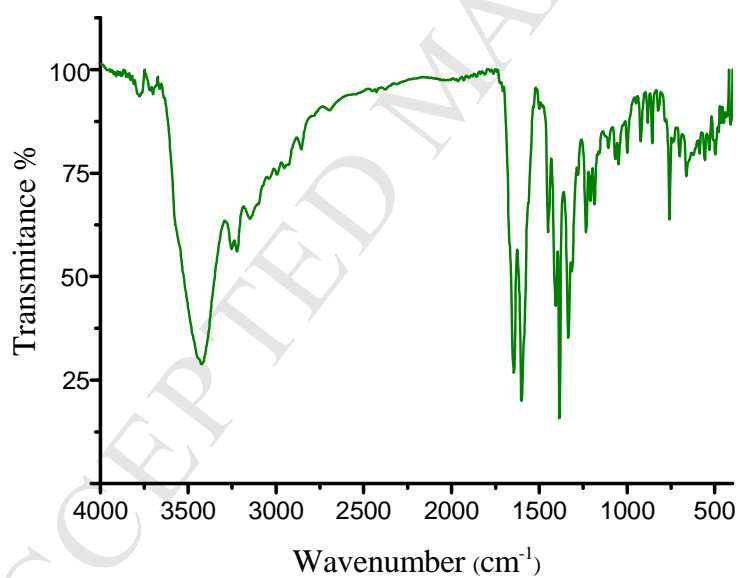


**Figure 3:** FTIR spectrum of compound 3-Ni.

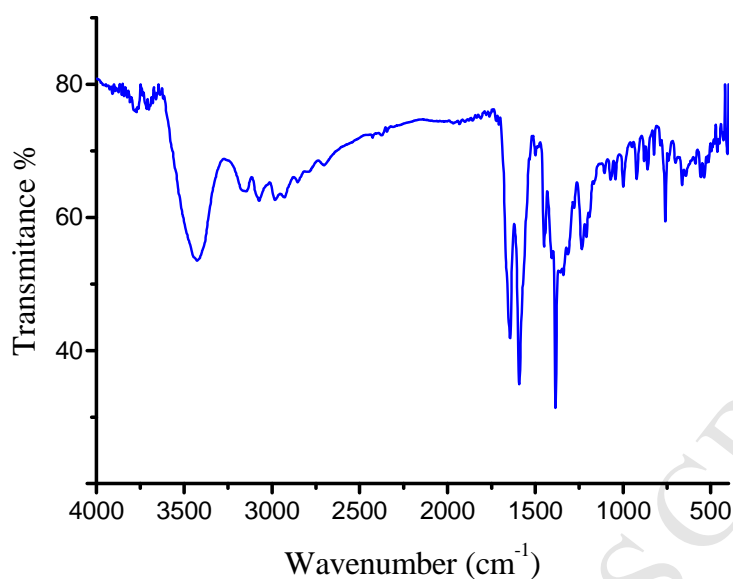


**Figure 4:** FTIR spectrum of compound **3-Cu**.

#### **3.4. Uv-Vis Spectra:**

The Uv-Vis absorption spectra which were produced due to the electronic transitions from the highest occupied molecular orbital (HOMO) to the lowest unoccupied molecular orbital (LUMO) [30], were carried out in ethanolic solution as listed in **Table 3** and showed in **Figures 5-8**.

Generally, the obtained spectra exhibit ligands bands due to  $\pi \rightarrow \pi^*$  and  $n \rightarrow \pi^*$  transitions, which in consequently undergo some red and blue shifts on complexation. The bathochromic (red) and hypochromic (blue) effect strongly revealed the formation of the target complexes. The d-d transition need extra elucidation due to the very small value of the molecular absorptivity ( $\epsilon$ ) of this type of transition [31,32].

#### **3.5. Magnetic measurements**

Magnetic susceptibilities of metal complexes were investigated by the Gouy method which involves weighing a sample of the complex in the presence and absence of a magnetic field and observing the difference in weight. The measurements were carried out using Sherwood Scientific's Magnetic Susceptibility Balance [22]. The mass magnetic susceptibility ( $X_g$ ) was calculated by

$$X_g = LC(R - R_0) / m \times 10^9$$

Where **L** = sample length in centimeters

**m** = sample mass in grams

**C** = balance calibration constant (printed on the back of the instrument)

**R** = reading from the digital display when the sample (in the sample tube) is in the balance.

**R<sub>0</sub>** = reading from the display when the empty sample tube is in the balance

The number of unpaired electrons was evaluated by magnetic susceptibility, where paramagnetic metal complexes arise inherent magnetic moment from the spins of unpaired electrons. The effective magnetic moment value of metal complex,  $\mu_{\text{eff}}$ , was given by the sum of spin moments:

$$\mu_{\text{eff}} = \mu_{\text{spin}} = \sqrt{4s(s+1)} = \sqrt{n(n+2)}$$

where spin moments  $S = 1/2 n$  and  $n$  is the number of unpaired electrons [33,34].

Also, the effective magnetic moment was calculated from the molar susceptibility by the following equation:

$$\mu_{\text{eff}} = 2.83 \sqrt{X_M \cdot T}$$

where  $X_M$  is the molar susceptibility which equal mass susceptibility multiplied by mole weight and  $T$  is the absolute temperature [35–37].

The magnetic moment measurements of metal complexes are given in **Table 3**. The Cu (II) complexes (**2-Cu**, **3-Cu**, **1-Cu** and **4-Cu**) have magnetic moment value lying in the range of the planar structure. Ni(II) and Co(II) complexes have magnetic moment value in the range of the octahedral structure (**Table 3**).

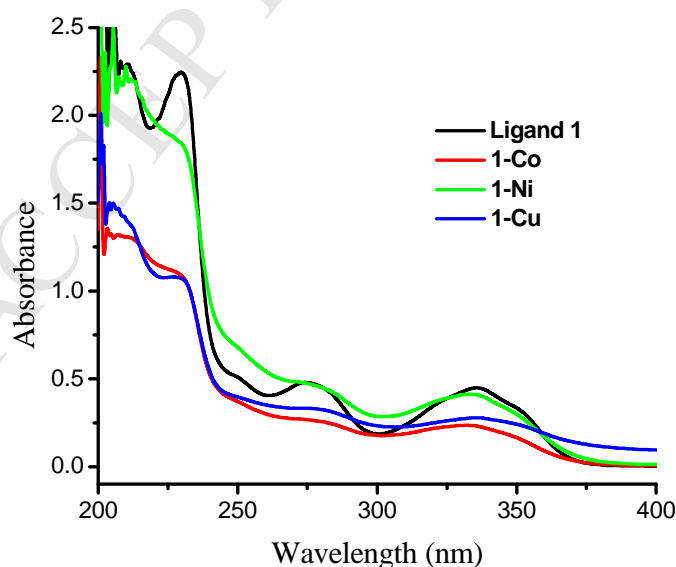


**Figure 5:** Uv-Vis spectra of the ligand **1** and its complexes.

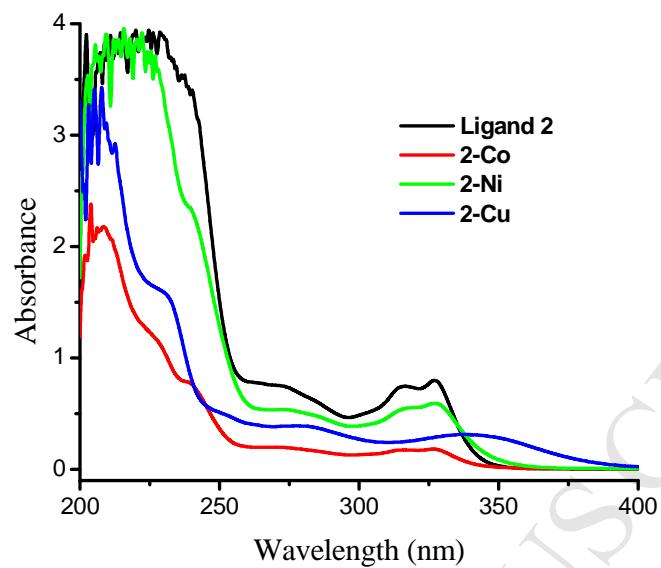


**Figure 6:** Uv-Vis spectra of the ligand **2** and its complexes.

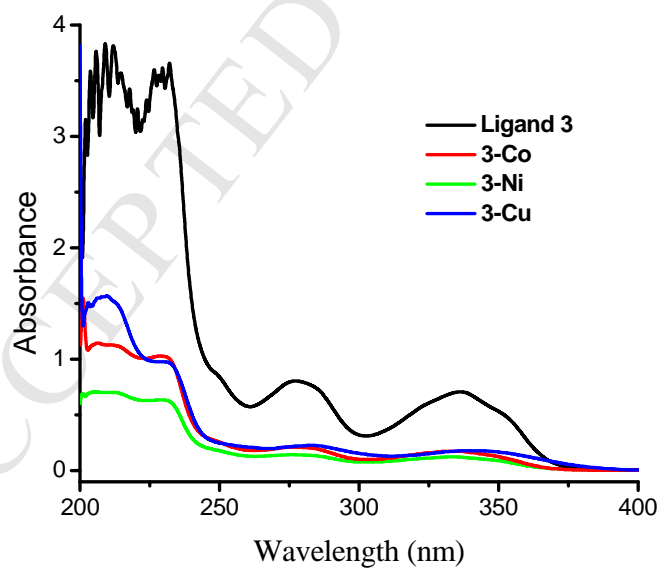


**Figure 7:** Uv-Vis spectra of ligand **3** and its complexes.

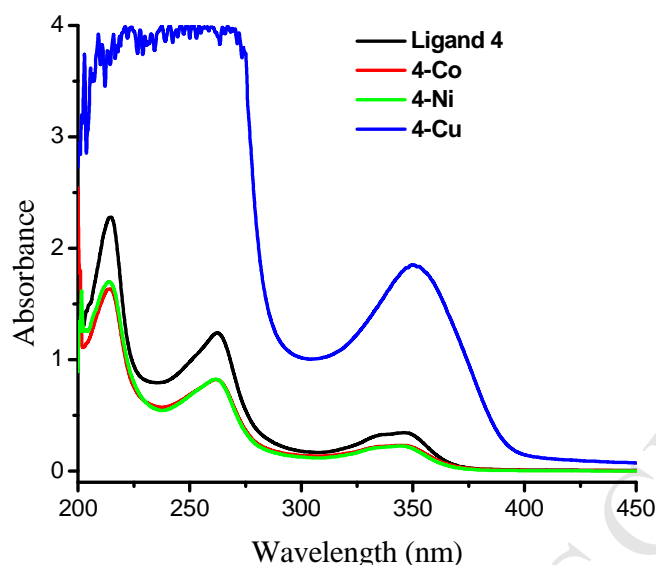


**Figure 8:** Uv-Vis spectra of ligand **4** and its complexes.

### 3.6. Thermal analysis

The target complexes were subjected to TG-DTA analysis in ambient temperature up to 800 °C under nitrogen atmosphere. The decomposition temperature ranges, the percentage of mass losses and the thermal effects accompanying the decomposition process are given in **Table 4–7**. Representative thermal curves TG/DTG-DTA of the complexes under consideration are given in **Figures 9-11** as representative examples and the remaining figure is presented in a supplementary file.

The thermal decomposition behavior of the complexes derived from ligand **1** was listed in **Table 4**. The obtained metal % goes well with the postulated complexes formula and the residual product was found as MO structure. The thermal decomposition of the **1-Ni** was proceeding through three steps; meanwhile **1-Cu** and **1-Co** were carried out through four steps. The water of crystallization was liberated at DTA temperature= 62 °C for **1-Cu** as endothermic behavior with weight loss revealed two moles of water. Water of coordination was liberated with the same exothermic behavior for **1-Ni** and **1-Co** complexes. The weight loss in TG analysis indicates liberation 2H<sub>2</sub>O. The thermal decomposition of the ligand proceeds through two steps for all target complexes. The first decomposition step has the following trend: **1-Co** > **1-Ni** > **1-Cu** with exothermic behavior (**Table 4**).

The TGA/DTG and DTA thermogram of the complexes derived from ligand **2** are listed in **Table 5**. The **2-Cu** complex was thermally decomposed through different steps, where the first step starts at 40 °C and finished at 100 °C accompanied with DTA peak as endothermic one at 77 °C. The weight loss accompanied with step, according to the TG diagram= 9.82, which go well with the calculated value

which obtained from the liberation of 4 molecules from water, which classified as water of crystallization. The ligand decomposition was preceded through exothermic peaks start at 173 °C. Also, liberation of the nitrate group carried out with exothermic peaks. The residue % goes well with the calculated value of the CuO %. The **2-Ni** complex liberates the two molecules from coordinated water at temperature range finished at 135 °C. The ligand decomposition start decomposed at DTA peak= 150 °C. The residue % goes well with the calculated value as NiO moiety. **2-Co** complex resemble the thermal decomposition behavior of the **2-Ni** complex, where the coordinated water liberated with weight loss % enhanced the liberation of two molecules of water. The residue % indicates the presence of the CoO moiety [38,39]. From the obtained data, the results could be summarized as follows:

- **2-Cu** gave thermal decomposition behavior different from the **2-Ni** and **2-Co**, meanwhile **2-Ni**  $\approx$  **2-Co**.
- The thermal stability of the coordinated water of **2-Ni** > **2-Co**.
- The residual product for all complexes was MO (M = Cu, Ni and Co).

The TGA/DTG and DTA thermogram of the complexes derived from ligand **3** are listed in **Table 6**. Generally, the thermal decomposition of the target complexes goes well with the same thermal process. The liberation of the water of crystallization was carried out at DTA peak temperature= 120 °C for the **3-Cu** complex with endothermic behavior. The thermal stability of the ligand in the target complex has the following trend: **3-Co** > **3-Ni** > **3-Cu**. The thermal stability of the nitrate group in the complexes has the following trend: **3-Cu** > **3-Co** > **3-Ni**. The residual % was going well with the postulated product formula MO (**Table 6**).

The thermal decomposition behavior of the complexes derived from ligand **4** was listed in **Table 7**. The obtained data revealed the distinguishable properties of this ligand more than the other. Each complex nearly has the special thermal decomposition trend. **4-Co** complex gave the largest numbers of decomposition steps meanwhile **4-Cu** the lowest. The liberation of the water of crystallization need energy has the following trend: **4-Ni**  $\approx$  **4-Co**. The TG analysis indicates the liberation of 2H<sub>2</sub>O for **4-Ni** and 4H<sub>2</sub>O for **4-Co** complex. The thermal decomposition of the coordinated water has the following stability trend: **4-Ni** > **4-Co**. The residual % of **4-Cu** strongly indicates the complicated thermal decomposition process of this complex; meanwhile **4-Ni** and **4-Co** go well with the MO formula. The principle difference of ligand **4** with the other ligand, is the presence of Sulphur atom in its structure, which could play a different role in thermal reactions (**Table 7**) [40,41].

According to the elemental analysis, conductivity, Uv/Vis spectra, FTIR, magnetic susceptibility and thermal analysis (DTA/TGA), could formulate obtained complexes as shown in Schemes 2-5.

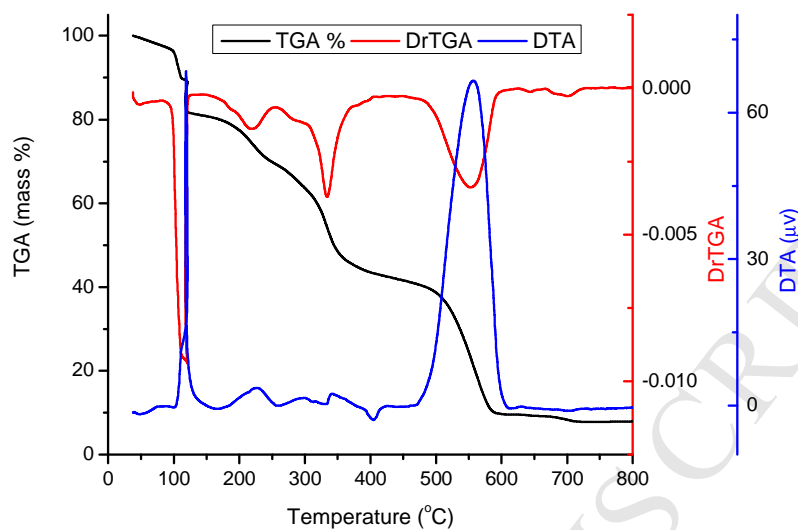


**Figure 9:** The thermogram of the DTA/TG analysis of the Complex **4-Co**.

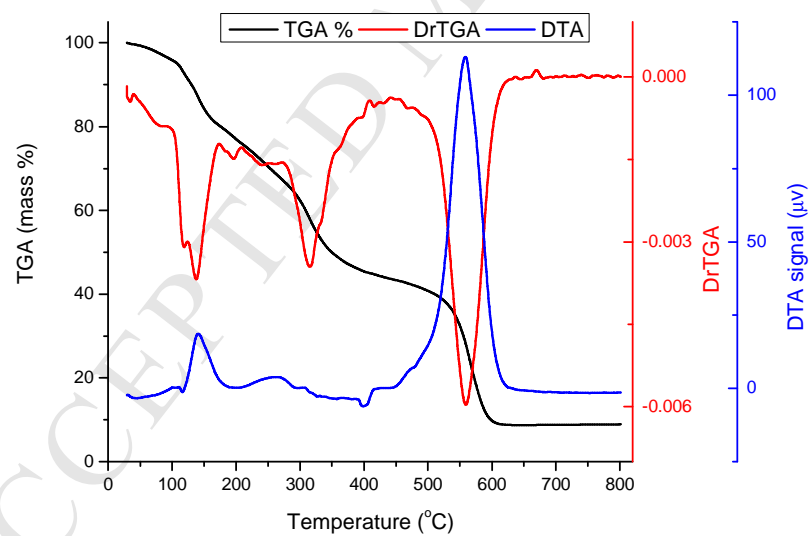


**Figure 10:** The thermogram of the DTA/TG analysis of the Complex **4-Ni**.

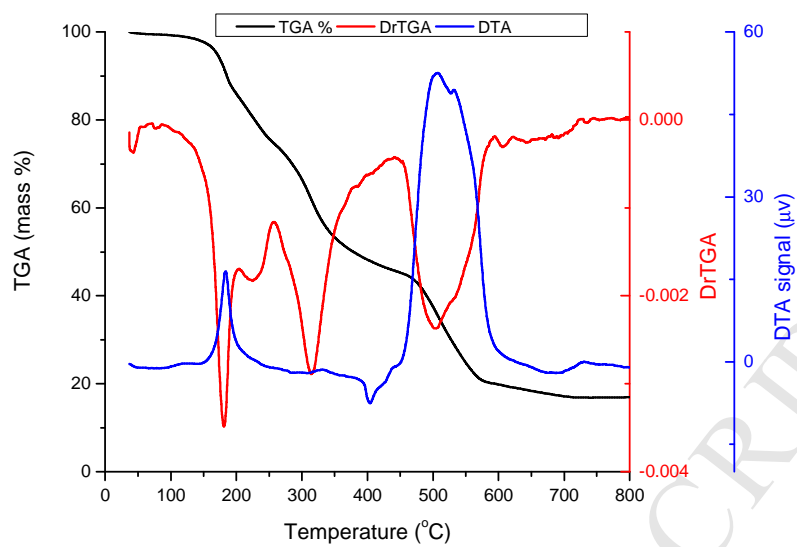


**Figure 11:** The thermogram of the DTA/TG analysis of the Complex **4-Cu**.

**Table 1:** The physico-chemical properties of the target ligands and their complexes

Compound	Formula	M.wt.	Color	m.p	Elemental analysis				Conductivity $\Omega$ ( $\mu\text{S}$ ) <sup>a</sup>
					N%		M%		
					C.	F.	C.	F.	
1	$\text{C}_{10}\text{H}_9\text{N}_3\text{O}_2$	203.20	Beige	>300	20.68	20.90	-	-	-
1-Cu	$[\text{Cu}(\text{C}_{10}\text{H}_9\text{N}_3\text{O}_2)_2](\text{NO}_3)_2 \cdot (\text{H}_2\text{O})_2$	629.98	Green	283	17.79	17.66	10.09	9.98	140
1-Ni	$[\text{Ni}(\text{C}_{10}\text{H}_9\text{N}_3\text{O}_2)_2(\text{H}_2\text{O})_2](\text{NO}_3)_2$	625.13	Ice blue	298	17.93	17.87	9.39	9.50	155
1-Co	$[\text{Co}(\text{C}_{10}\text{H}_9\text{N}_3\text{O}_2)_2(\text{H}_2\text{O})_2](\text{NO}_3)_2$	625.37	Cream	290	17.92	17.70	9.42	9.36	160
2	$\text{C}_{13}\text{H}_{13}\text{N}_3\text{O}_2$	243.27	White	166	17.27	17.30	-	-	-
2-Cu	$[\text{Cu}(\text{C}_{13}\text{H}_{13}\text{N}_3\text{O}_2)_2](\text{NO}_3)_2 \cdot (\text{H}_2\text{O})_4$	746.14	Green	110	15.02	15.21	8.52	8.37	166
2-Ni	$[\text{Ni}(\text{C}_{13}\text{H}_{13}\text{N}_3\text{O}_2)_2(\text{H}_2\text{O})_2](\text{NO}_3)_2$	705.26	Green	170	15.89	15.95	8.32	8.64	170
2-Co	$[\text{Co}(\text{C}_{13}\text{H}_{13}\text{N}_3\text{O}_2)_2(\text{H}_2\text{O})_2](\text{NO}_3)_2$	705.50	Brown	135	15.88	15.63	8.35	8.22	173
3	$\text{C}_{13}\text{H}_{13}\text{N}_3\text{O}_2$	243.27	Yellow	267	17.27	17.13	-	-	-
3-Cu	$[\text{Cu}(\text{C}_{13}\text{H}_{13}\text{N}_3\text{O}_2)_2](\text{NO}_3)_2 \cdot (\text{H}_2\text{O})_2$	710.11	Turquoise	292	15.78	15.92	8.95	8.72	151
3-Ni	$[\text{Ni}(\text{C}_{13}\text{H}_{13}\text{N}_3\text{O}_2)_2(\text{H}_2\text{O})_2](\text{NO}_3)_2$	705.26	Ice blue	270	15.89	15.71	8.32	8.11	177
3-Co	$[\text{Co}(\text{C}_{13}\text{H}_{13}\text{N}_3\text{O}_2)_2(\text{H}_2\text{O})_2](\text{NO}_3)_2$	705.50	Orange	218	15.88	15.79	8.35	8.40	169
4	$\text{C}_{13}\text{H}_{13}\text{N}_3\text{OS}$	259.33	Beige	156	16.20	16.29	-	-	-
4-Cu	$[\text{Cu}(\text{C}_{13}\text{H}_{13}\text{N}_3\text{OS})_2](\text{NO}_3)_2$	706.22	Brown	160	15.87	15.61	9.00	8.79	160
4-Ni	$[\text{Ni}(\text{C}_{13}\text{H}_{13}\text{N}_3\text{OS})_2(\text{H}_2\text{O})_2](\text{NO}_3)_2 \cdot (\text{H}_2\text{O})_2$	773.42	Brown	106	14.49	14.58	7.59	7.56	169
4-Co	$[\text{Co}(\text{C}_{13}\text{H}_{13}\text{N}_3\text{OS})_2(\text{H}_2\text{O})_2](\text{NO}_3)_2 \cdot (\text{H}_2\text{O})_4$	809.69	Brown	140	13.84	13.61	7.28	7.33	179

M.wt.= molecular weight    m.p= melting point    C= calculated    F= found    <sup>a</sup>  $10^{-3}$  M in DMSO,  $\text{ohm}^{-1} \cdot \text{cm}^2 \cdot \text{mol}^{-1}$

**Table 2:** The most effective IR spectra of the target ligands and their complexes

Comp.	$\nu_{\text{O-H}}$	$\nu_{\text{N-H}}$	$\nu_{\text{C=O}}$	$\nu_{\text{NO}_3}$	$\nu_{\text{M-O}}$	$\nu_{\text{M-N}}$
1	3438 br, m	3270 s 3202 sh	1653 s 1517 s	-	-	-
1-Cu	364-3354 br, s	3153 m	1653 s 1582 sh	1381 s	657	514
1-Ni	3638-2649 br, s		1672 s, br 1622 s, br 1562 s	1381 s	528 w	476 w
1-Co	3645-2675 br, s		1672 br, s 1622 br, s 1562 s	1381 s	528 w	468 w
2	3454 s, br	3277 s	1640 m 1604 s	-	-	-
2-Cu	3632-2700 s, br		1659 s	1381 s	657 w	514 w
2-Ni	3665- 2765 s, br		1656 sh s 1582 sh, s	1394 s	630 w	520 w
2-Co	3651-2804 s, br		1692 sh 1656 s 1581 s	1396 s	586 w	520 w
3	3438 sh.br	3347 s 3270 s	1634 s 1581 s	-	-	-
3-Cu	3431 s, br	-	1646 s 1601 s	1388 s	553 w	540 w
3-Ni	3425 s, br	324 w 3258 w	1646 s 1600 s	1387 s	560 w	500 w
3-Co	3439 s, br	3233 w	1648 s 1600 s	1379 s	547 w	483 w
4	3438 br,s	3296 s	1627 s 1588 s	-	-	-
4-Cu	3625-3179 br, s		1633 sh 1607 s 1536 m	1387 s	608 w	553 w
4-Ni	3651-3088 br, s		1640 sh 1595 sh, m 1543 sh, m	1381 s	598 w	489 w
4-Co	3632-3036 br, m		1633 sh 1585 sh, m 1543 sh, m	1381 s	602 w	489 w

s= strong m= medium w= weak sh= shoulder br= broad

**Table 3:** The magnetic and electronic spectra of the ligands and their complexes

Comp.	$n \rightarrow \pi^*$ and $\pi \rightarrow \pi^*$ transition	$\mu_{\text{eff}}$ (B.M)	Postulated Structure	Hybrid orbitals	n
1	335, 277, 250, 229	-	-	-	-
1-Cu	334, 279, 228	1.96	Planar	$\text{dsp}^2$	1
1-Ni	332, 275, 229	2.98	Octahedral	$\text{sp}^3\text{d}^2$	2
1-Co	332, 275, 227	4.87	Octahedral	$\text{sp}^3\text{d}^2$	3
2	327, 315, 273	-	-	-	-
2-Cu	341, 277, 227	1.80	Planar	$\text{dsp}^2$	1
2-Ni	327, 315, 273, 239	3.30	Octahedral	$\text{sp}^3\text{d}^2$	2
2-Co	327, 314, 275, 240, 224	5.20	Octahedral	$\text{sp}^3\text{d}^2$	3
3	336, 277, 250	-	-	-	-
3-Cu	343, 231, 208	1.91	Planar	$\text{dsp}^2$	1
3-Ni	334, 276, 230, 210	3.51	Octahedral	$\text{sp}^3\text{d}^2$	2
3-Co	334, 280, 230, 207	4.92	Octahedral	$\text{sp}^3\text{d}^2$	3
4	347, 334, 263, 214	-	-	-	-
4-Cu	350	1.82	Planar	$\text{dsp}^2$	1
4-Ni	342, 261, 214	3.25	Octahedral	$\text{sp}^3\text{d}^2$	2
4-Co	342, 261, 214	5.08	Octahedral	$\text{sp}^3\text{d}^2$	3

**Table 4:** The thermal analysis data for the synthesized ligand **1** and its complexes

Comp.	Temp. range (°C)	DTA peak temp. (°C)	Peak Type	Mass loss %		Process	Expected products	Residue% Found (Calcd.)
				Found	Calcd.			
<b>1-Cu</b>	30-105	62	Endo.	5.50	5.72	Water of crystallization	2H <sub>2</sub> O	12.00 (12.63) CuO
	105-205	175	Exo.	52.00	51.61	Partial ligand decomposition	0.8 L	
	205-378	347	Exo.	13.00	12.90	Partial ligand decomposition	0.2 L	
	378-504	432	Exo.	20.00	4.68	Liberation of NO <sub>3</sub>	NO <sub>3</sub>	
<b>1-Ni</b>	50-225	225	Exo.	5.00	5.76	Water of coordination	2H <sub>2</sub> O	11.60 (11.95) NiO
	225-239	234	Exo.	32.00	32.51	Partial ligand decomposition	0.5 L	
	239-447	443	Exo.	52.40	52.35	Ligand decomposition +Liberation of NO <sub>3</sub>	0.5 L + NO <sub>3</sub>	
<b>1-Co</b>	187-215	207	Exo.	-	5.76	Water of coordination	2H <sub>2</sub> O	11.40 (11.98) CoO
	215-266	262	Exo.	12.83	13.00	Partial ligand decomposition	0.2 L	
	266-433	397	Exo.	33.00	32.50	Partial ligand decomposition	0.5 L	
	433-449	435	Exo.	39.6	39.33	Ligand decomposition + Liberation of NO <sub>3</sub>	0.3 L + NO <sub>3</sub>	

L= Total ligand content

**Table 5:** The thermal analysis data for the synthesized ligand **2** and its complexes

Comp.	Temp. range (°C)	DTA peak temp. (°C)	Peak Type	Mass loss %		Process	Expected products	Residue% Found (Calcd.)
				Found	Calcd.			
<b>2-Cu</b>	40-100	77	Endo.	9.82	9.66	Water of crystallization	4H <sub>2</sub> O	11.50 (10.66) CuO
	100-252	173	Exo.	32.00	32.61	Partial ligand decomposition	0.5 Ligand	
	252-473	318	Exo.	49.00	49.23	Ligand decomposition + liberation of NO <sub>3</sub>	0.5 Ligand + NO <sub>3</sub>	
		333	Exo.					
		340	Exo.					
424		Exo.						
<b>2-Ni</b>	55-135	-	-	5.00	5.11	Water of coordination	2H <sub>2</sub> O	10.00 (10.59) NiO
	135-158	150	Exo.	53.00	53.00	Partial ligand decomposition	0.77 Ligand	
	158-513	392	Exo.	33.50	33.57	Ligand decomposition + liberation of NO <sub>3</sub>	0.23 Ligand + NO <sub>3</sub>	
		423	Exo.					
<b>2-Co</b>	50-123	-	-	5.00	5.11	Water of coordination	2H <sub>2</sub> O	11.50 (10.62) CoO
	123-176	166	Exo.	68.50	68.96	Ligand decomposition	Ligand	
	176-459	262	Exo.	18.00	17.58	Liberation of NO <sub>3</sub>	NO <sub>3</sub>	
		298	Exo.					
		404	Exo.					
Exo.								

L= Total ligand content

**Table 6:** The thermal analysis data for the synthesized ligand **3** and its complexes

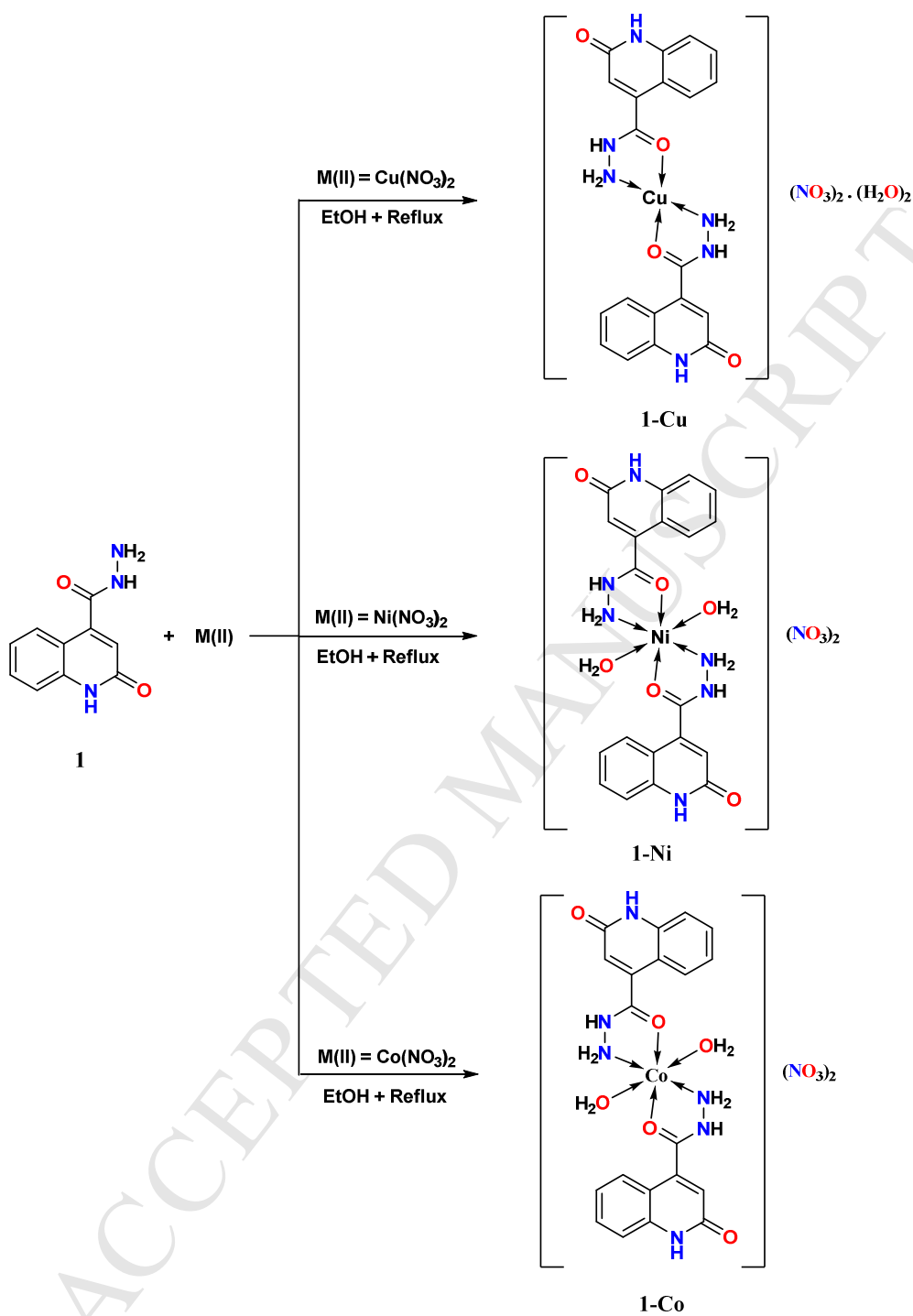
Comp.	Temp. range (°C)	DTA peak temp. (°C)	Peak Type	Mass loss %		Process	Expected products	Residue% Found (Calcd.)
				Found	Calcd.			
<b>3-Cu</b>	40-147	120	Endo.	5.00	5.07	Water of crystallization Ligand decomposition Liberation of NO <sub>3</sub>	2H <sub>2</sub> O	10.50 (11.20) CuO
	147-44	181	Exo.	68.00	68.51		L	
	44-497	436	Exo.	17.00	17.46		NO <sub>3</sub>	
<b>3-Ni</b>	50-132	-	-	5.00	5.11	Water of coordination	2H <sub>2</sub> O	11.00 (10.59) NiO
	132-151	139	Exo.	69.00	68.99	Ligand decomposition	L	
	151-529	343	Exo.	18.00	17.58	Liberation of NO <sub>3</sub>	NO <sub>3</sub>	
		376	Exo.					
		477	Exo.					
<b>3-Co</b>	50-203	128	Endo.	5.00	5.11	Water of coordination	2H <sub>2</sub> O	10.00 (10.62) CoO
	203-239	223	Exo.	69.50	68.96	Ligand decomposition	L	
	239-423	357	Exo.	17.50	17.58	Liberation of NO <sub>3</sub>	NO <sub>3</sub>	

L= Total ligand content

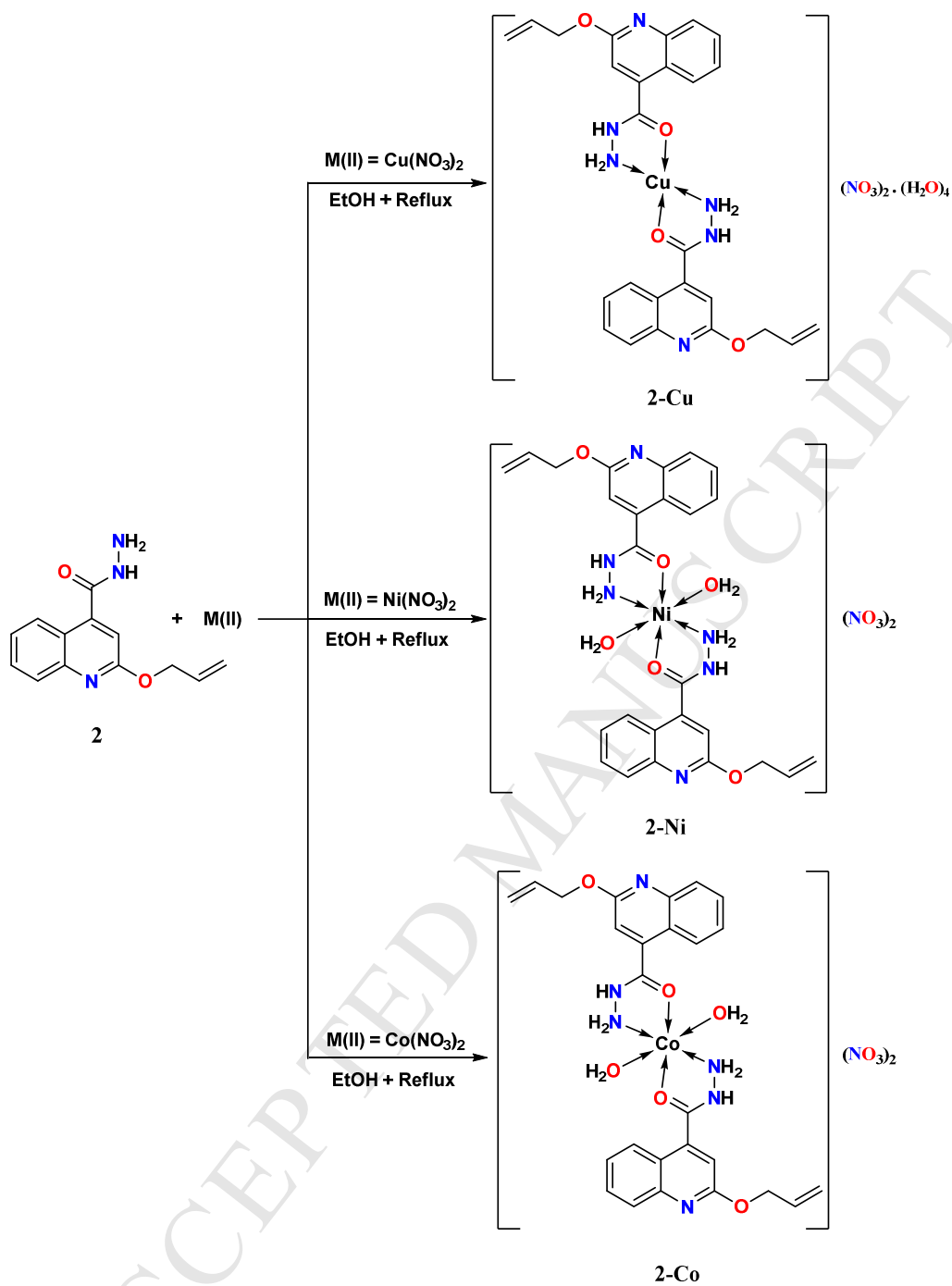
**Table 7:** The thermal analysis data for the synthesized ligand **4** and its complexes

Comp.	Temp. range (°C)	DTA peak temp. (°C)	Peak Type	Mass loss %		Process	Expected products	Residue% Found (Calcd.)
				Found	Calcd.			
<b>4-Cu</b>	40-273	184	Exo.	28.00	27.91	Partial ligand decomposition	0.38 L	22.00
	273-475	402	Endo.	30.00	30.11	Partial ligand decomposition	0.41 L	CuS (13.54)
	475-588	505	Exo.	18.00	17.56	Liberation of NO <sub>3</sub>	NO <sub>3</sub>	CuO (11.26)
<b>4-Ni</b>	32-112	106	Exo.	5.00	4.66	Water of crystallization	2H <sub>2</sub> O	10.00
	112-155	142	Exo.	5.50	4.66	Water of coordination	2H <sub>2</sub> O	(9.66)
	155-380	261	Exo.	38.00	37.55	Partial ligand decomposition	0.56 L	NiO
	380-620	558	Exo.	35.00	34.81	Ligand decomposition + liberation of NO <sub>3</sub>	0.28 L + NO <sub>3</sub>	
<b>4-Co</b>	50-108	-	-	9.00	8.90	Crystallization Water	4H <sub>2</sub> O	9.00
	108-130	14	Exo.	5.00	4.45	Coordination Water	2H <sub>2</sub> O	(9.25)
	130-279	225	Exo.	12.00	12.17	Partial ligand decomposition	0.4 L	CoO
	279-436	340	Exo.	26.00	26.26	Partial ligand decomposition	0.41 L	
	436-624	557	Exo.	32.00	31.98	Ligand decomposition + liberation of NO <sub>3</sub>	0.26 L + NO <sub>3</sub>	

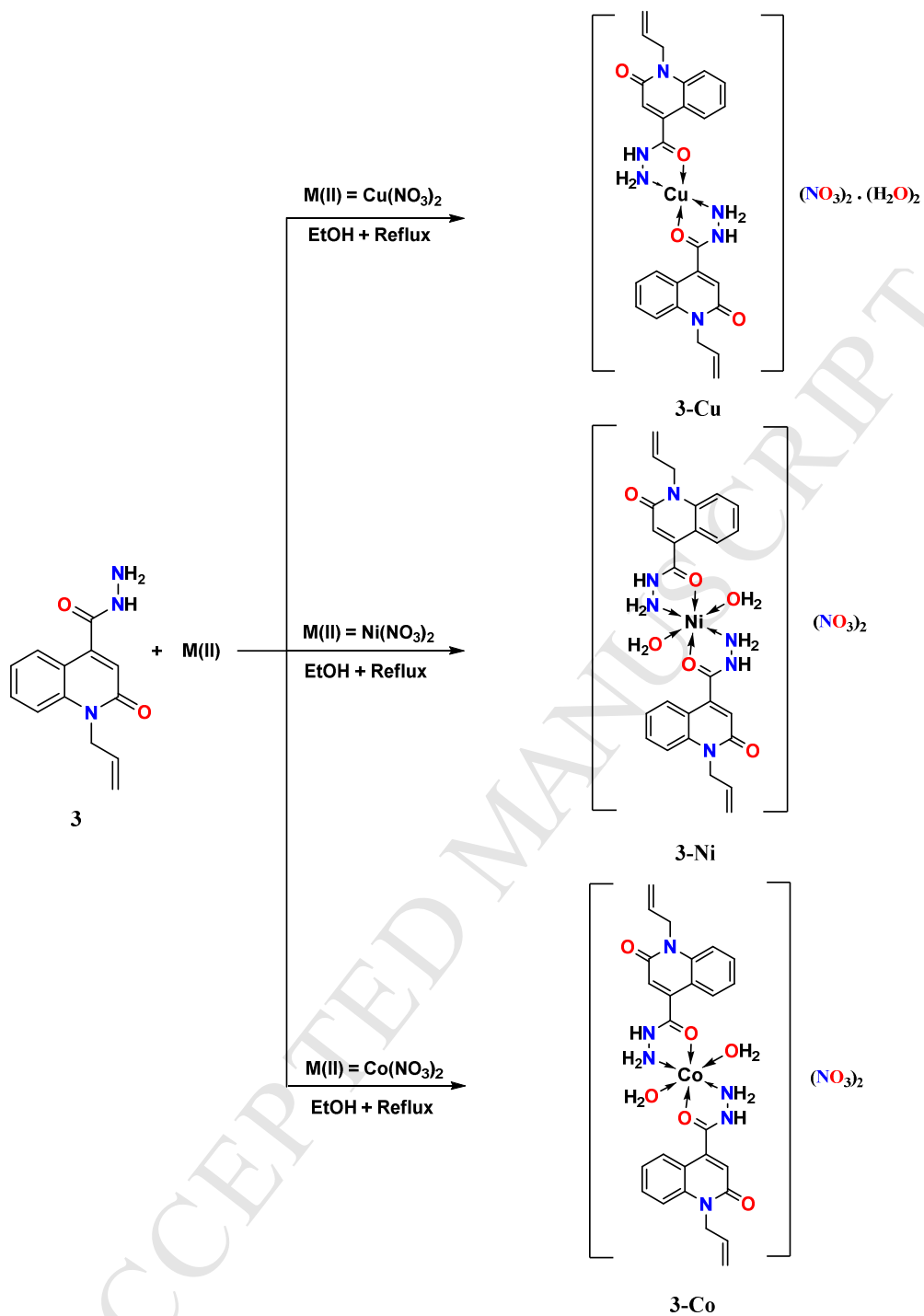
L= Total ligand content



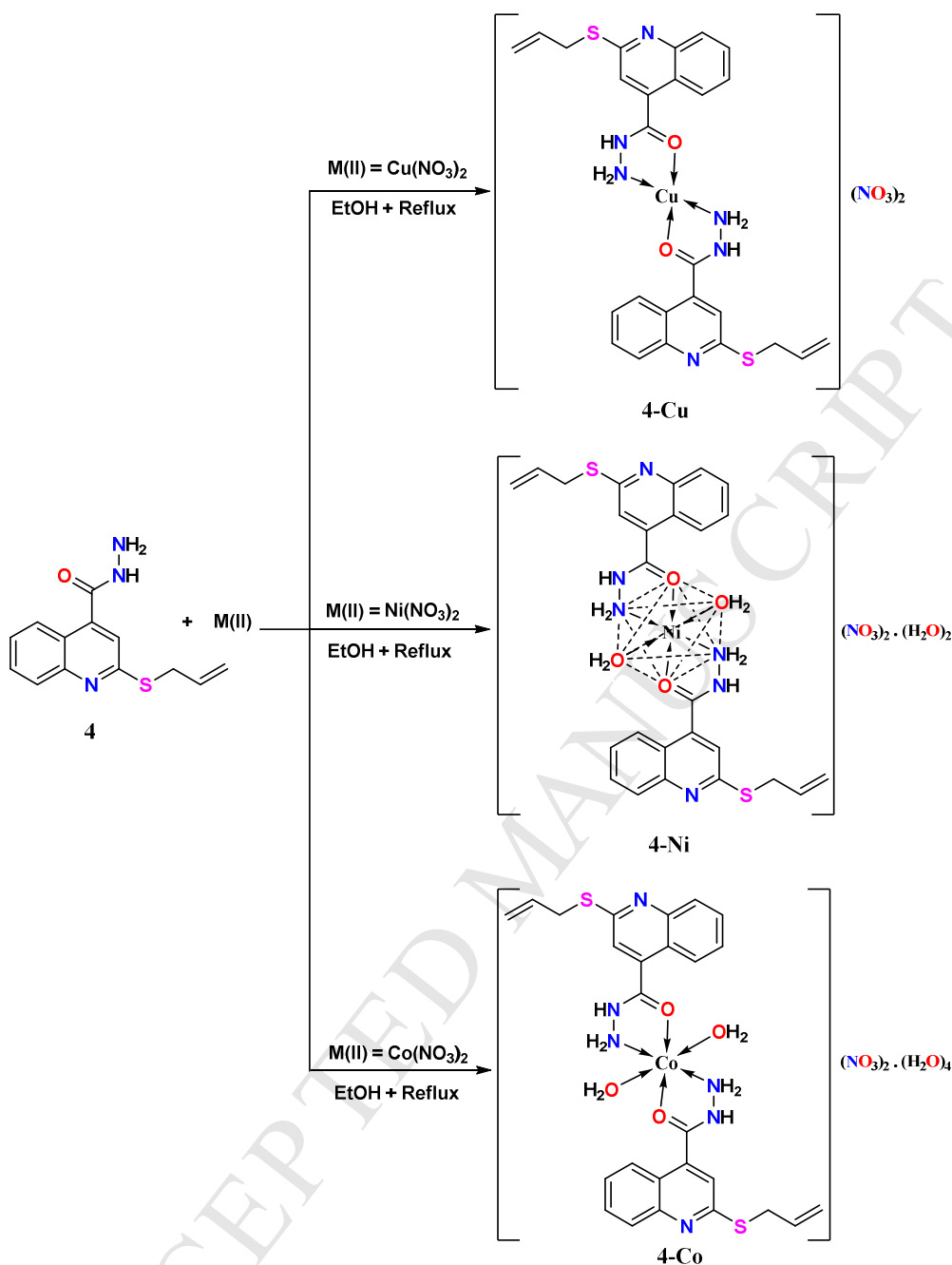
**Scheme 2:** The postulated structure of the metal complexes of the ligand **1**



**Scheme 3:** The postulated structure of the metal complexes of the ligand **2**



**Scheme 4:** The postulated structure of the metal complexes of the ligand **3**



**Scheme 5:** The postulated structure of the metal complexes of ligand **4**

### 3.7. The Density Function Theory (DFT)

The DFT was carried out to calculate and explore the effect of HOMO and LUMO energy on the compounds which were previously calculated in MM2 level (as representative examples for the thesis compounds). Each studied compound was undergoing energy minimization using the force field parameter MMFF94x. The simulation process was carried out using SCF (self-consistent field method, also named Hartree–Fock method) calculation. MOPAC system was used with Hamiltonian PM3 using RHF (restricted Hartree-Fock method).

### 3.7.1. The Density Function Calculation for Compound 1

As shown in **Figure 12** and listed in **Table 8**, the application of the DFT on compound **1** gave representative data. The electron density map indicates the cylindrical density on the aromatic rings with branched chain nearly present out of plan of aromatic rings. The density= 0 at the center of the rings (**Figure 12.B**). The view of the electron density map plays an important role in selecting the receptor in the drug design process. The  $\pi$ - $\pi$  stacking and interaction could be proceeded through the rich electron density poses [42–44]. The HOMO and LUMO orbitals gave some hints about the target orbitals which were involved in the electronic migration process that was intricate in the excitation–relaxation pathway. The large number of occupied and unoccupied orbitals revealed the lower energy which needed to promote electron from one level to another. The energy of the HOMO, LUMO and  $\Delta E$  was listed in **Table 8**. The dipole value (4.00 D) indicates the polarity of compound **1**, which is unfavorable for drug behavior [45].

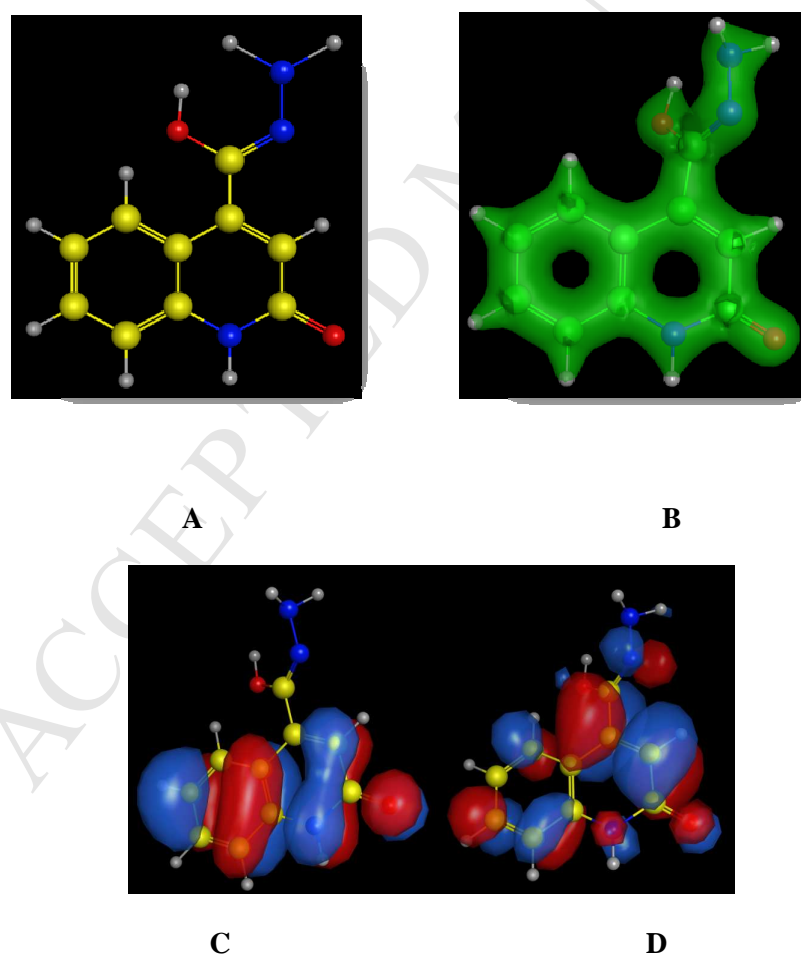
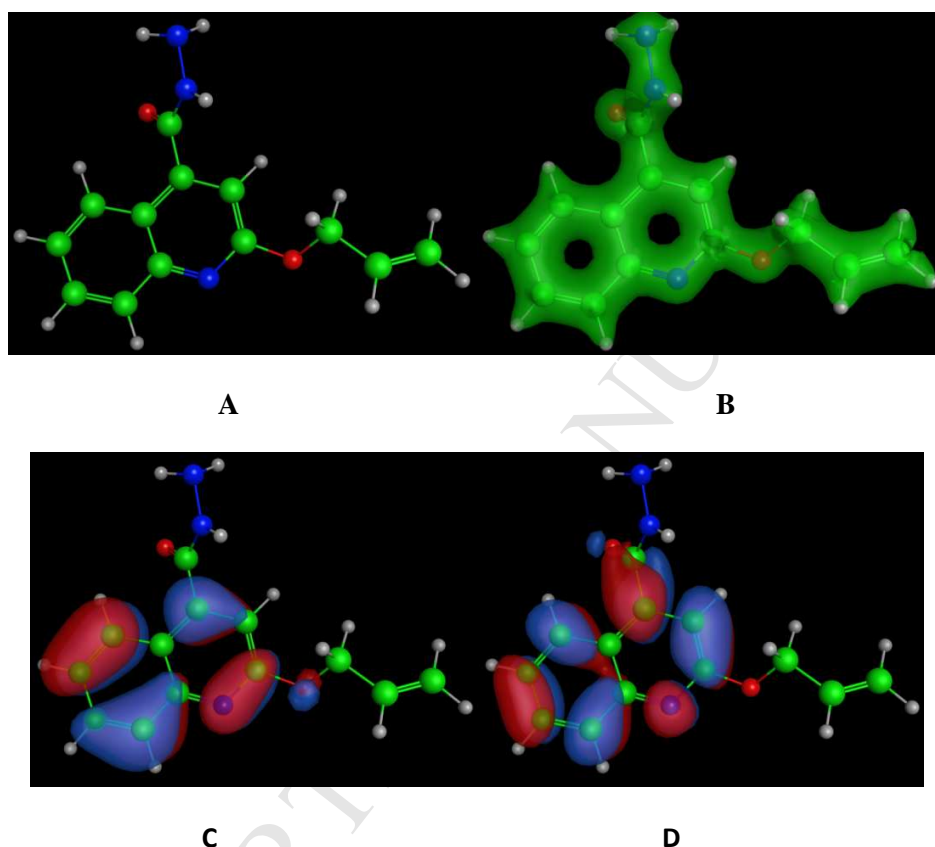


**Figure 12:** The DFT simulation for the compound **1**

[A] 3D view, [B] Electron density map, [C] HOMO and [D] LUMO

### 3.7.2. The Density Function Calculation for Compound 2

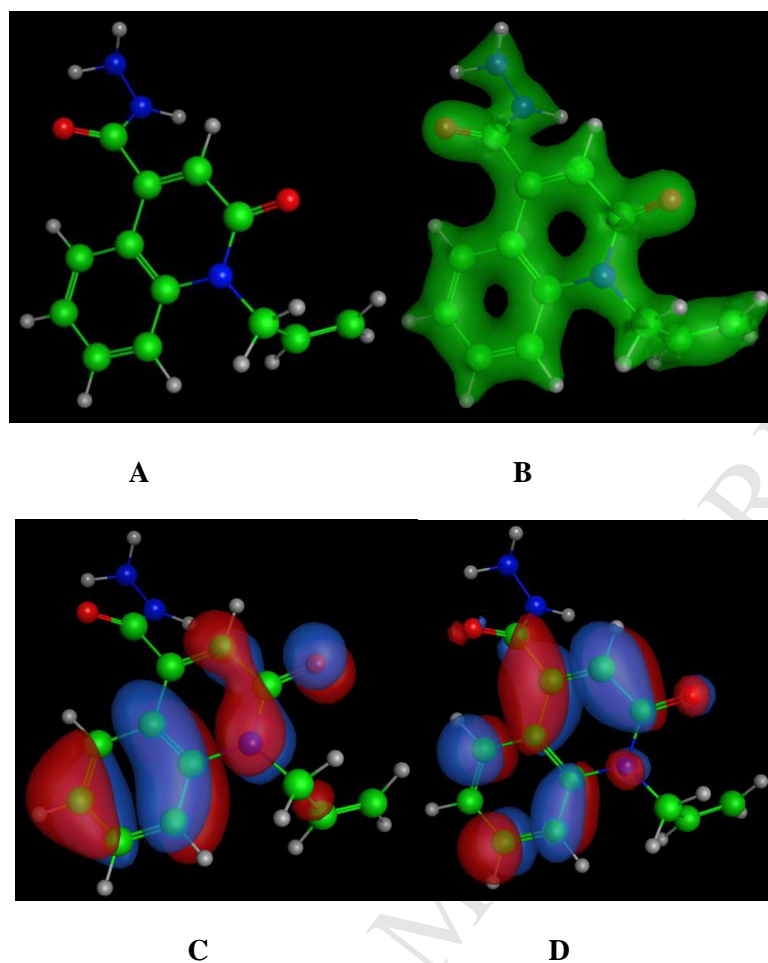
The application of the DFT on compound **2** gave the data, shown in **Figure 13** and listed in **Table 8**. The dipole value (2.71 D) goes well with the requirement properties of the new drug [45]. Compound **2** was comparable to compound **3**. Both compounds have a large number of orbitals and electrons which revealed the existence of a large number of poses that could interact with the receptor. Thus, the value of being a drug is enhanced. [42–44].



**Figure 13:** The DFT simulation for compound **2**, [A] 3D view, [B] Electron density map, [C] HOMO and [D] LUMO

### 3.7.3. The Density Function Calculation for Compound 3

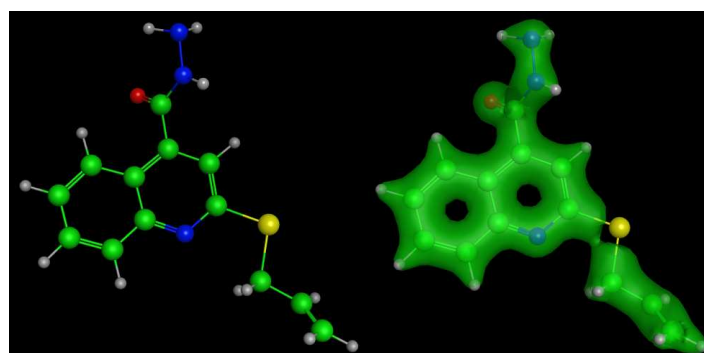
The application of the DFT on compound **3** gave a representative data, as shown in **Figure 14** and listed in **Table 8**. The dipole value (2.89 D) goes well with the requirement properties of the new drug [45]. Compound **3** has larger atoms, orbitals and electrons than those of compound **1**. These differences can predict some variation in their energy [42–44]. The electron density map of compound **3** clearly indicated the existence of a more branched area other than that of compound **1**. Indeed, this added other poses for interaction with receptor, and accordingly, enhanced the potency of the drug [45].



**Figure 14:** The DFT simulation for compound **3**, [A] 3D view, [B] Electron density map, [C] HOMO and [D] LUMO

#### 3.7.4. The Density Function Calculation for Compound 4

The application of the DFT on compound **4** gave the data shown in **Figure 15** and listed in **Table 8**. The dipole value (1.73 D) goes well with the requirement properties of the new drug [45]. The large number of orbitals and electrons revealed the presence of a large number of poses that could interact with the receptor, enhancing its opportunity for being a drug [42–44].



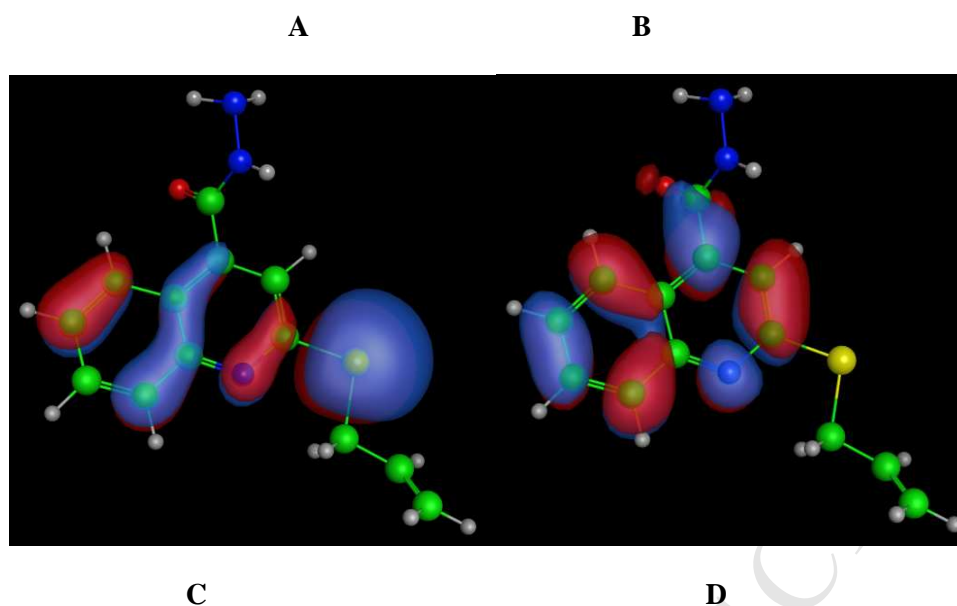


**Figure 15:** The DFT simulation for compound **4**, [A] 3D view, [B] Electron density map, [C] HOMO and [D] LUMO

A profound assessment of the target compounds, with respect to their energy and the accompanied properties, can be summarized in the following obtained results:

1. The SCF energy:  $3 \approx 2 > 4 > 1$
2. Dipole:  $1 > 3 > 2 > 4$
3.  $E_{\text{LUMO}}$ :  $1 > 3 > 2 > 4$
4.  $E_{\text{HOMO}}$ :  $4 > 1 > 3 > 2$
5.  $E_{\text{HOMO-LUMO}}$ :  $1 > 3 > 2 > 4$
6. The electron affinity (A):  $4 > 2 > 3 > 1$
7. Electronegativity ( $\chi$ ):  $2 > 4 > 3 > 1$
8. Global hardness ( $\eta$ ):  $1 > 3 > 2 > 4$

**Table 8:** The DFT simulation data for the synthesized compounds

	<b>1</b>	<b>2</b>	<b>3</b>	<b>4</b>
<b>Formula</b>	C <sub>10</sub> H <sub>9</sub> N <sub>3</sub> O <sub>2</sub>	C <sub>13</sub> H <sub>13</sub> N <sub>3</sub> O <sub>2</sub>	C <sub>13</sub> H <sub>13</sub> N <sub>3</sub> O <sub>2</sub>	C <sub>13</sub> H <sub>13</sub> N <sub>3</sub> OS
<b>Atoms</b>	24	31	31	31
<b>Orbitals</b>	69	85	85	85
<b>Electrons</b>	76	92	92	92
<b>SCF energy</b>	-88.043 au	-103.324 au	-103.347 au	-99.384 au
<b>Dipole</b>	4.00 D	2.71 D	2.89 D	1.73 D
<b>E<sub>LUMO</sub></b>	-0.033 au -0.901 eV	-0.048 au -1.296 eV	-0.037 au -1.000 eV	-0.051 au -1.396 eV
<b>E<sub>HOMO</sub></b>	-0.330 au -8.978 eV	-0.334 au -9.082 eV	-0.332 au -9.026 eV	-0.325 au -8.844 eV
<b>ΔE<sub>HOMO-LUMO</sub></b>	0.297 au 8.077 eV 153.49 nm	0.286 au 7.786 eV 159.23 nm	0.295 au 8.026 eV 154.47 nm	0.274 au 7.448 eV 166.45 nm
<b>I (I.E)</b>	8.978	9.082	9.026	8.844
<b>A (electron affinity)</b>	0.901	1.296	1.000	1.396
<b>χ (electronegativity)</b>	4.940	5.189	5.013	5.120
<b>η (global hardness)</b>	4.039	3.893	4.013	3.724

### 3.8. In Vitro and In Silico Antimicrobial Activity

#### [A] Antimicrobial Activity of Compound 1 and its Complexes

The obtained data which listed in **Table 9** and presented in **Figure 16** revealed the promising activity towards the tested Gram positive and Gram negative bacterial also with the target fungi. The obtained data could be summarized as the following:

1. Compound **1** gave the lowest activity towards the target microorganism.
2. Generally Cu (II) complex gave the largest activity which exceeding the market drug.
3. Ni (II) and Co (II) complexes are nearly close to each other in their activity.
4. The synthesized compounds have large activity toward the target bacteria rather than the target fungi.
5. All the complexes have larger activity than that of the parent ligand.
6. The target complexes have a competitive force with the reference market drug (Ampicillin).

7. The order of activity towards the *E. Coli*: **1-Cu > Ampicillin > 1-Ni > 1-Co > 1 > Fluconazole.**
8. The order of activity towards the *B. Subtilis* is: **1-Cu > Ampicillin > 1-Co > 1-Ni > 1 > Fluconazole.**
9. The order of activity towards the *Asp. Niger* is: **Fluconazole > 1-Cu > 1-Co > 1-Ni > 1 > Ampicillin.**

The variation among the activities of the target complexes could be associated with the structure of the obtained complexes, where Cu (II) complex has a square planar structure, while Ni (II) and Co (II) has octahedral structure, as mention previously.

The interaction of the target compounds with the tested microorganism was simulated and evaluated by using the *in Silico* tools. The *E. Coli* was used as an example of the target microorganism. The protein which was used for docking process was 5C9T. The data which was represented in **Table 9** and **Figure 17**, strongly forced the obtained activities. The strong interaction of the synthesized compounds with the target protein could either enhance or hinder the activity of the protein. The docking was carried out using triangle matcher method with rescoring = London dG with force field refinement.

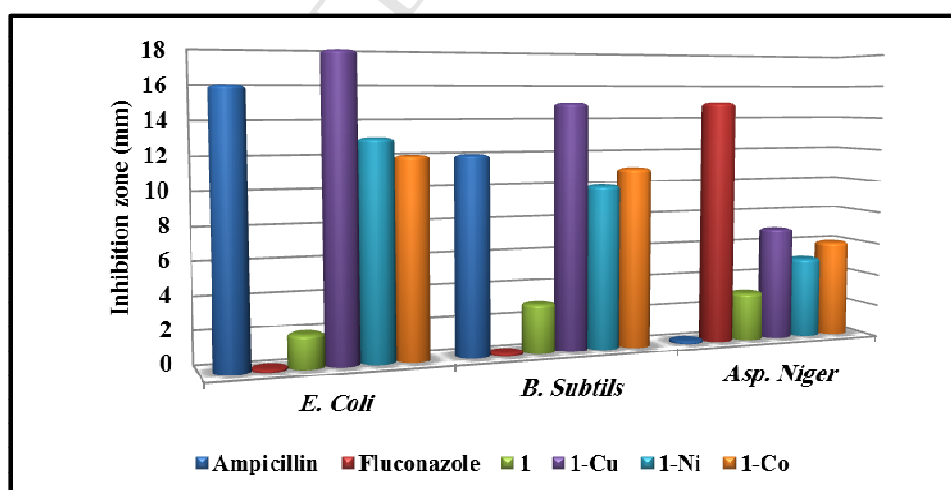
In working case, the activity was strongly retarded as the compound bonded strongly with the protein, with the exception of compound **1**. Cu (II) complex bonded with the target protein by 5 bonds, while Co (II) by 3 bonds. Also, the mode of the interaction plays some role about the antimicrobial activity, which clearly shown as 2D docking view for the target compounds in **Figure 17**.

**Table 9:** Docking and antimicrobial data for compound **1** and its complexes

Comp.	Inhibition zone (mm) <sup>a</sup>			No. of bonds	Bond type	Bond energy <sup>b</sup>	Binding energy <sup>b</sup>
	<i>E. Coli</i>	<i>B. Subtils</i>	<i>Asp. Niger</i>				
Ampicillin	16 ± 1	12 ± 1	0.2 ± 1	6	HD HA HA HA HA HA	6.10 -3.20 -2.20 -5.30 -2.20 -0.80	66.110
Fluconazole	0	0.2 ± 0.5	15 ± 2	5	HD HA HA Pi-cation Pi-H	-0.80 -5.50 -4.40 -2.20 -0.70	50.975
1	2 ± 1	3 ± 0.5	3 ± 0.6	4	HD HD HA Pi-H	-1.10 -2.50 -0.60 -1.20	-5.759
1-Cu	18 ± 2	15 ± 0.8	7 ± 0.5	5	HD HD HA HA ionic	-1.80 -1.20 -1.10 -0.03 -2.10	91.499
1-Ni	13 ± 1	10 ± 1	5 ± 0.8	4	HD HD HA ionic	-5.60 -1.20 -1.20 -2.70	130.065
1-Co	12 ± 0.7	11 ± 0.5	6 ± 1	3	HA HA ionic	2.90 25.20 -3.40	204.838

a = well diameter = 6 mm

b = kcal/mol

**Figure 16:** The antimicrobial behavior of the compound **1** and its complexes.

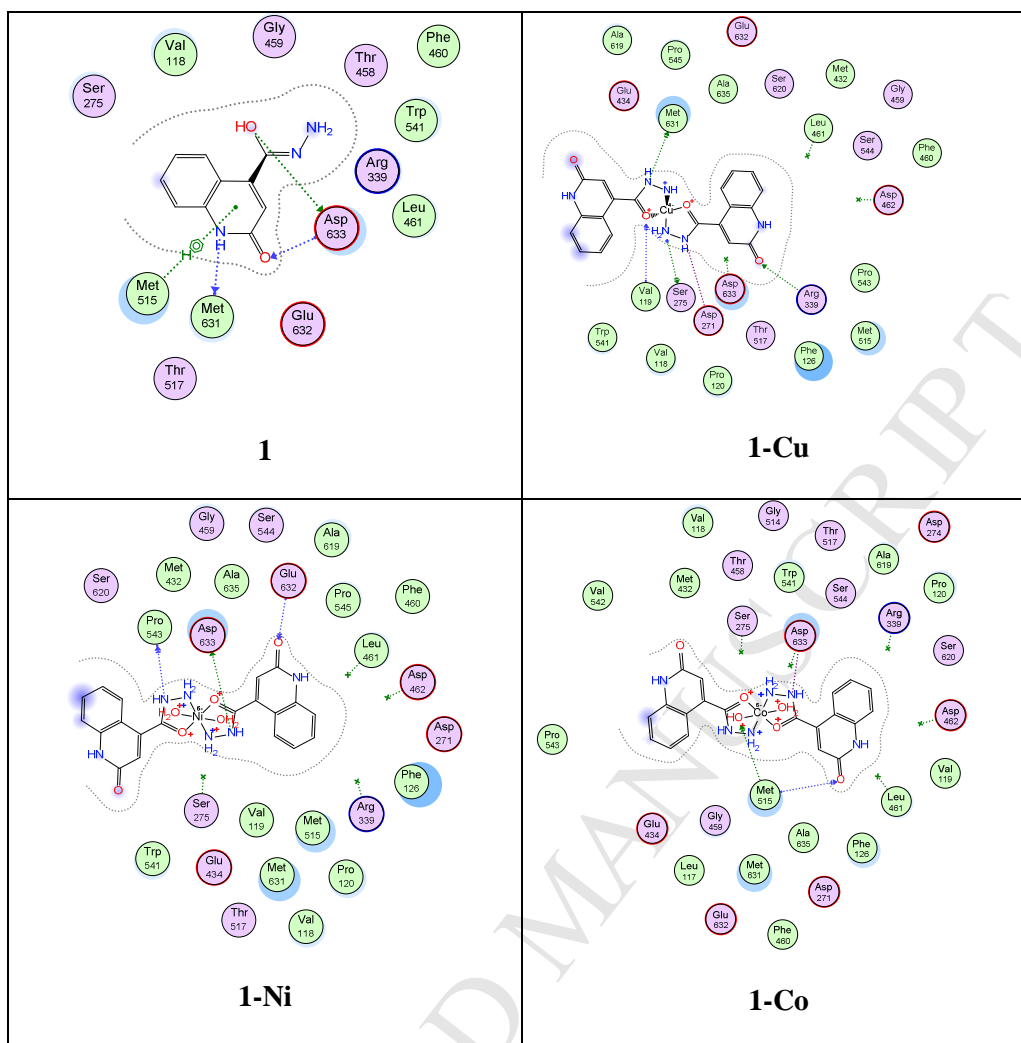


**Figure 17:** Docking model of the interaction of compound **1** and its complexes with *E. Coli* (PDB code **5C9T**) as 2D view.

[B] Antimicrobial activity of compound **2** and its complexes

The obtained data, which is listed in **Table 10** and presented in **Figure 18**, revealed the moderate activity towards the tested Gram positive and Gram negative bacterial as well as the target fungi. The obtained data could be summarized as follows:

1. Compound **2** gave the lowest activity towards the target microorganism.
2. Generally Cu (II) complex gave the largest activity among the complexes.
3. Ni (II) and Co (II) complexes are nearly close to each other in their activity.
4. The synthesized compounds have large activity toward the target Gram –ve bacteria rather than the Gram +ve and fungi.
5. All the complexes have larger activity than the parent ligand
6. The order of activity towards the *E. Coli* is:

**Ampicillin > 2-Cu > 2-Ni > 2-Co > 2 > Fluconazole**

7. The order of activity towards the *B. Subtilis* is:

**Ampicillin > 2-Cu > 2-Ni > 2-Co > 2 > Fluconazole**

8. The order of activity towards the *Asp. Niger* is:

**Fluconazole > 2-Cu > 2-Co > 2-Ni > 2 > Ampicillin**

The variation among the activities of the target complexes could be interrelated with the structure of the obtained complexes, where Cu (II) complex has square planar structure while Ni (II) and Co (II) have an octahedral structure, as mention previously.

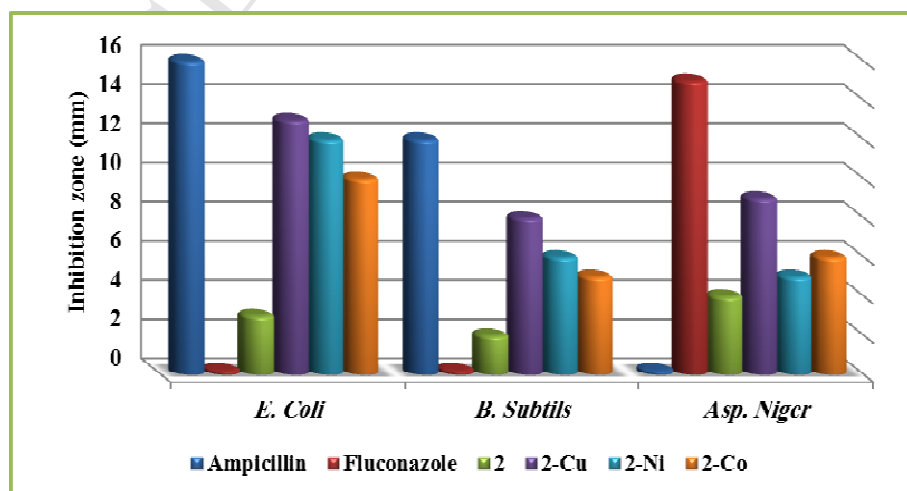
The interaction of the target compounds with the tested microorganism was simulated and evaluated by using *in Silico* tools. The *E. Coli* (protein code 5C9T) was used as an example of the target microorganism. Table II-4.8 showed that, the Cu (II) and Ni (II) complexes have 6 bonds with the target protein, whereas Co (II) has 3 bonds. The mode of interaction was fitted in **Figure 19** as 2D view.

**Table 10:** Docking and antimicrobial data for compound **2** and its complexes:

Comp.	Inhibition zone (mm) <sup>a</sup>			No. of bonds	Bond type	Bond energy <sup>b</sup>	Binding energy <sup>b</sup>
	<i>E. Coli</i>	<i>B. Subtils</i>	<i>Asp. Niger</i>				
Ampicillin	16 ± 1	12 ± 1	0.2 ± 1	6	HD HA HA HA HA HA	6.10 -3.20 -2.20 -5.30 -2.20 -0.80	66.110
Fluconazole	0	0.2 ± 0.5	15 ± 2	5	HD HA HA Pi-cation Pi-H	-0.80 -5.50 -4.40 -2.20 -0.70	50.975
2	3 ± 0.8	2 ± 0.5	4 ± 1	4	HD HD HD HA	-3.90 -2.40 -1.70 -1.60	36.020
2-Cu	13 ± 1	8 ± 0.8	9 ± 1	6	HD HD HD Ionic Pi-H Pi-pi	-0.90 -1.70 -1.60 -1.80 -0.70 -0.02	146.022
2-Ni	12 ± 1	6 ± 1	5 ± 1	6	HD HD HA Pi-H Pi-pi Pi-pi	-1.50 -0.80 -0.50 -0.70 -0.03 -0.03	147.450
2-Co	10 ± 2	5 ± 1	6 ± 2	3	HD HA ionic	-4.60 -0.03 -1.90	223.462

a = well diameter = 6 mm

b = kcal/mol

**Figure 18:** The antimicrobial behavior of the compound **2** and its complexes.

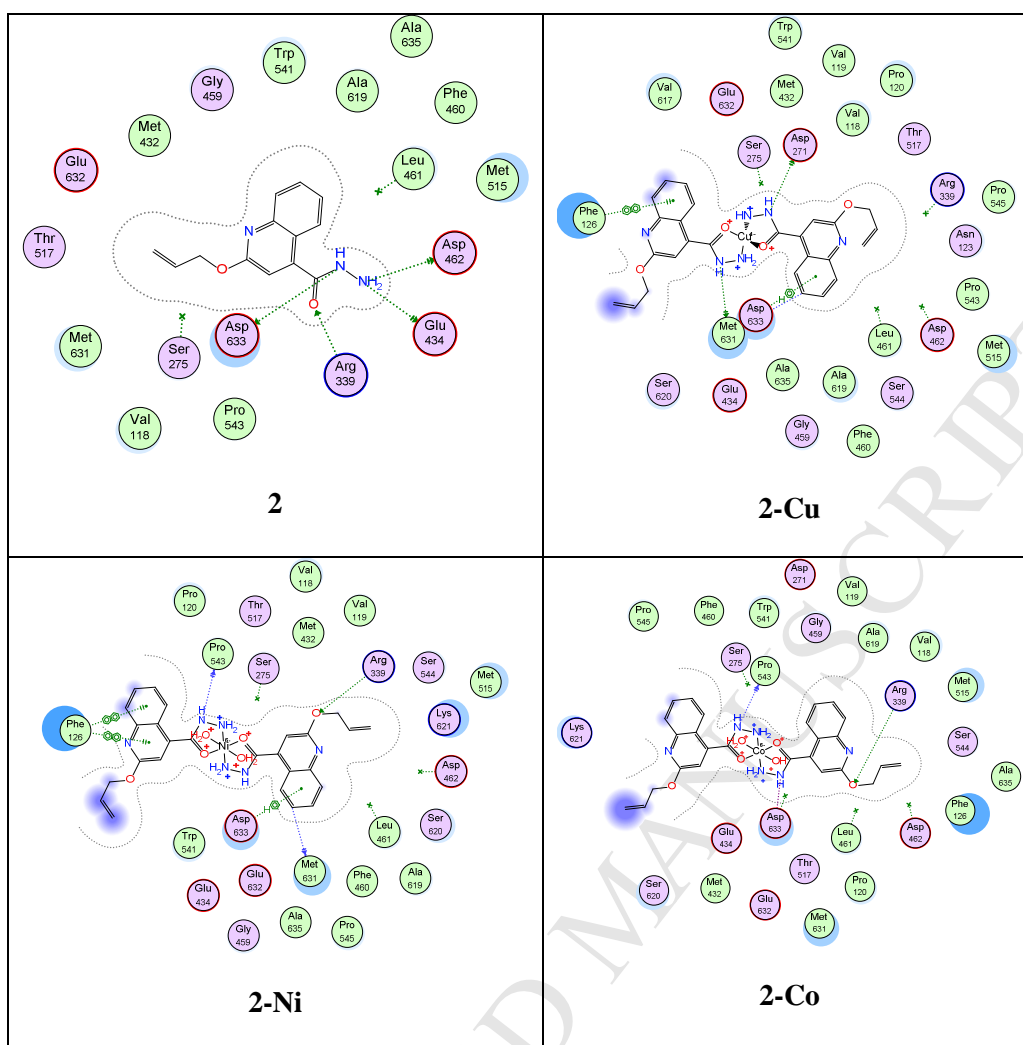


**Figure 19:** Docking model of the interaction of compound **2** and its complexes with *E. Coli* (PDB code **5C9T**) as 2D view.

[C] Antimicrobial activity of compound 3 and its complexes

The obtained data, which is listed in **Table 11** and presented in **Figure 20**, revealed the promising activity towards the tested Gram positive and Gram negative bacterial and a moderate activity toward the target fungi. The obtained data could be summarized as follows:

1. Compound **3** gave the lowest activity towards the target microorganism.
2. Generally, Cu (II) complex gave the largest activity, exceeding the market drug Ampicillin.
3. Co (II) complex are close to the market drug Ampicillin in their activities.
4. The synthesized compounds have a larger activity toward the target Gram –ve bacteria rather than the Gram +ve and fungi.
5. All the complexes have a larger activity than that of the parent ligand

6. The order of activity towards the *E. Coli* is: **3-Cu >Ampicillin =3-Co > 3-Ni >3> Fluconazole**
7. The order of activity towards the *B. Subtilis* is: **3-Cu >Ampicillin >3-Ni >3-Co >3> Fluconazole**
8. The order of activity towards the *Asp. Niger* is: **Fluconazole >3-Cu =3-Co >3-Ni >3> Ampicillin**

The variation among the activities of the target complexes could be referred to the structure of the obtained complexes, where Cu (II) complex has a square planar structure while Ni (II) and Co(II) have an octahedral structure, as mention previously.

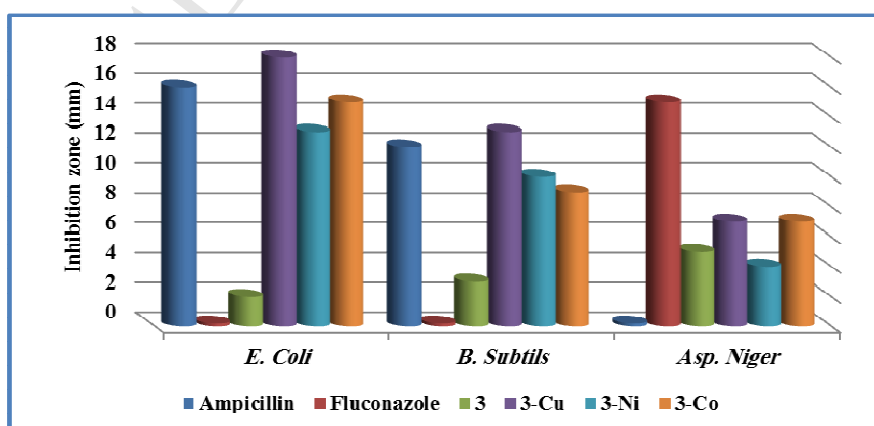
The interaction of the target compounds with the tested microorganism was simulated and evaluated by using the *in Silico* tools. The *E. Coli* (protein code 5C9T) was used as an example of the target microorganism. **Table 11** showed that, the Cu (II) complex has 8 bonds with the target protein while Co (II) has 5 bonds. The mode of interaction was fitted in **Figure 21** as 2D view. The docking data goes well with the *in vitro* antimicrobial activity.

**Table 11:** Docking and antimicrobial data for the compound **3** and its complexes:

Comp.	Inhibition zone (mm) <sup>a</sup>			No. of bonds	Bond type	Bond energy <sup>b</sup>	Binding energy <sup>b</sup>
	<i>E. Coli</i>	<i>B. Subtils</i>	<i>Asp. Niger</i>				
Ampicillin	16 ± 1	12 ± 1	0.2 ± 1	6	HD HA HA HA HA HA	6.10 -3.20 -2.20 -5.30 -2.20 -0.80	66.110
Fluconazole	0	0.2 ± 0.5	15 ± 2	5	HD HA HA Pi-cation Pi-H	-0.80 -5.50 -4.40 -2.20 -0.70	50.975
3	2 ± 0.6	3 ± 0.9	5 ± 0.9	4	HD HD HD Pi-H	-1.01 -1.01 -0.90 -2.20	35.774
3-Cu	18 ± 1	13 ± 0.5	7 ± 1	8	HD HD HD HA ionic Pi-H Pi-pi Pi-pi	-3.40 -0.80 -0.80 6.80 -0.60 -0.70 -0.03 -0.03	107.663
3-Ni	13 ± 0.8	10 ± 1	4 ± 1	4	HA HD Ionic H-pi	-5.20 0.40 -1.90 -0.80	140.902
3-Co	15 ± 0.9	9 ± 0.6	7 ± 1	5	HD HD HA H-pi Pi-cation	-0.70 -1.70 -0.80 -1.00 -0.60	204.342

a = well diameter = 6 mm

b = kcal/mol

**Figure 20:** The antimicrobial behavior of the compound **3** and its complexes.

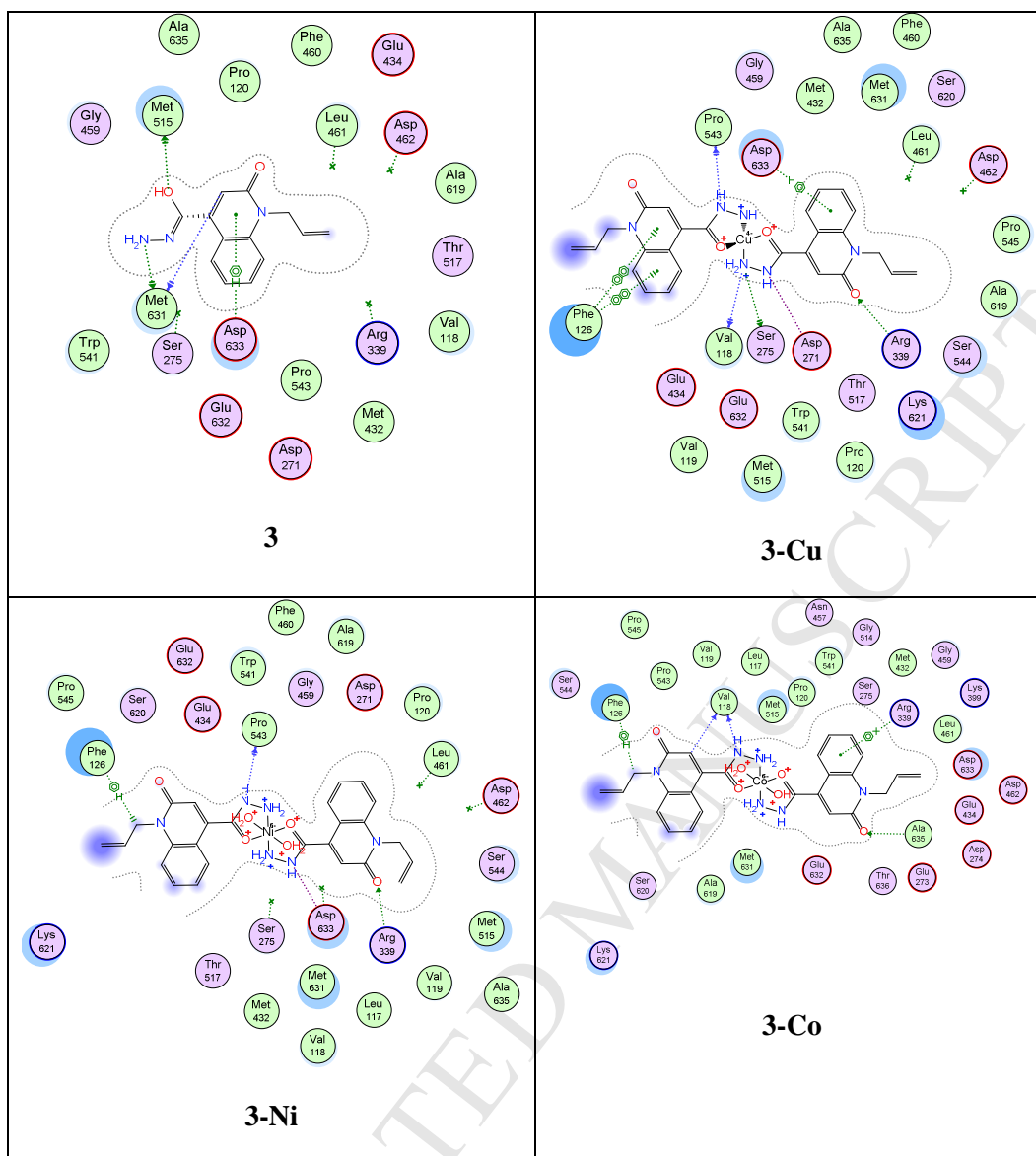


**Figure 21:** Docking model of the interaction of compound **3** and its complexes with *E. Coli* (PDB code **5C9T**) as 2D view.

[D] Antimicrobial activity of compound 4 and its complexes

The obtained data which was listed in **Table 12** and presented in **Figure 22** revealed the moderate activity towards the tested Gram positive, Gram negative bacterial and the target fungi. The obtained data could be summarized as follows:

1. Compound **4** gave the lowest activity towards the target microorganism.
2. Generally, Cu (II) complex gave the largest activity among the complexes.
3. Ni (II) and Co (II) complex are close to each other with respect to their activities towards the target bacteria.

4. The synthesized compounds have a large activity toward the target Gram –ve bacteria compared to the Gram +ve and fungi.
5. All the complexes have a larger activity than the parent ligand
6. The order of activity towards the *E. Coli* is:

**Ampicillin > 4-Cu > 4-Ni = 4-Co > 4 > Fluconazole**

7. The order of activity towards the *B. Subtilis* is:

**Ampicillin > 4-Cu > 4-Co > 4-Ni > 4 > Fluconazole**

8. The order of activity towards the *Asp. Niger* is:

**Fluconazole > 4-Cu > 4-Ni > 4-Co > 4 > Ampicillin**

The variation among the activities of the target complexes could be related to the structure of the obtained complexes, where Cu (II) complex has a square planar structure, whereas Ni (II) and Co(II) have an octahedral structure, as mention previously.

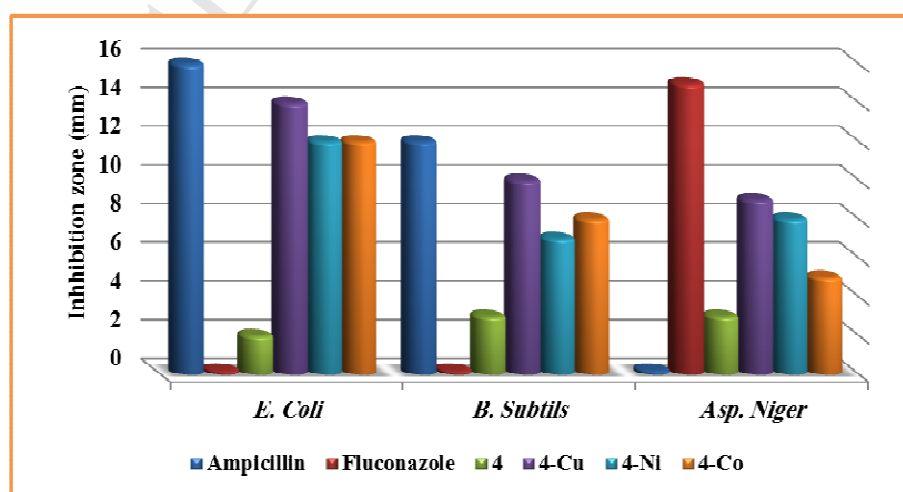
The interaction of the target compounds with the tested microorganism was simulated and evaluated by using the *in Silico* tools. The *E. Coli* ( protein code 5C9T) was used as an example for the target microorganism. The docking studies were performed after deleting the co-crystallized inhibitors from the active site. The active sites were defined by all the amino acid residues involved in the interaction with the co-crystallized inhibitors. **Table 12** showed that, the Cu (II) complex and its ligand have 6 bonds with the target protein while Ni(II) has 5 bonds and Co(II) has 4 bonds. The mode of interaction was fitted in **Figure 23** as 2D view. The docking data turn out well with the *in vitro* antimicrobial activity.

**Table 12:** Docking and antimicrobial data for the compound **4** and its complexes

Comp.	Inhibition zone (mm) <sup>a</sup>			No. of bonds	Bond type	Bond energy <sup>b</sup>	Binding energy <sup>b</sup>
	<i>E. Coli</i>	<i>B. Subtils</i>	<i>Asp. Niger</i>				
Ampicillin	16 ± 1	12 ± 1	0.2 ± 1	6	HD HA HA HA HA HA	6.10 -3.20 -2.20 -5.30 -2.20 -0.80	66.110
Fluconazole	0	0.2 ± 0.5	15 ± 2	5	HD HA HA Pi-cation Pi-H	-0.80 -5.50 -4.40 -2.20 -0.70	50.975
4	2 ± 0.4	3 ± 1	3 ± 1	6	HD HD HD HD HA Pi-H	-1.00 -0.02 -3.20 -1.10 44.90 -0.60	36.895
4-Cu	14 ± 0.8	10 ± 1	9 ± 0.8	6	HD HD ionic Pi-H Pi-pi Pi-pi	-3.90 -1.20 -0.80 -0.80 -0.03 -0.03	143.693
4-Ni	12 ± 0.9	7 ± 1	8 ± 0.9	5	HD HD HD HA ionic	-0.80 0.70 -2.90 0.20 -1.00	162.988
4-Co	12 ± 0.9	8 ± 0.8	5 ± 0.5	4	HD HD HD ionic	-0.70 -0.80 -4.10 -3.00	248.041

a = well diameter = 6 mm

b = kcal/mol

**Figure 22:** The antimicrobial behavior of the compound **4** and its complexes.

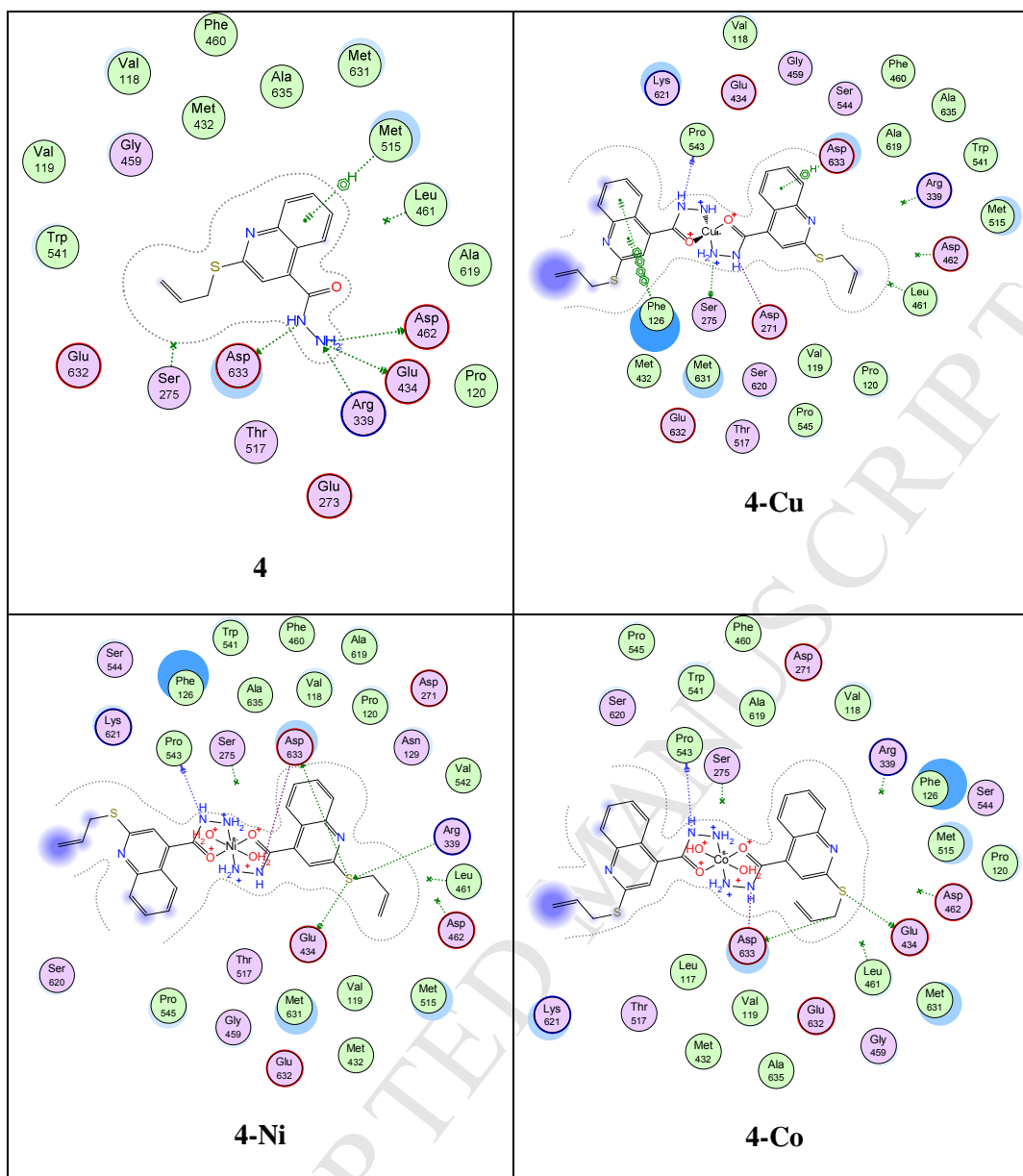


**Figure 23:** Docking model of the interaction of compound **4** and its complexes with *E. Coli* (PDB code 5C9T) as 2D view.

#### 4. Conclusion

The prepared compounds and their complexes were characterized by using different tools. The obtained data revealed the clear and pure products.

DFT calculations gave dipole order for the synthesized compounds as the following: **1** > **3** > **2** > **4**. The dipole of compound **4** = 1.73 proves to be suitable for drugs. Compounds which contain S atom (**4**), gave the largest electron affinity and minimum  $E_{\text{HOMO-LUMO}}$ . This characteristic indicates the effectiveness of this compound as a chemo-sensor.

The obtained data for the *In Vitro* antimicrobial activity revealed the promising activity towards the tested Gram positive and Gram negative bacterial as well as with the target fungi. Cu (II) complexes prove to be more vigorous than the ampicillin as a reference market drug.

The interaction of the target compounds with the tested microorganism was simulated and evaluated by using the *in Silico* tools. The *E. Coli* was used as an example of the target microorganism. 5C9T was used as a protein for the docking process.

The Cu (II) complex gave greater antibacterial activity than the market drug Ampicillin. Accordingly, it is recommended to be used as antibiotic drug, after pharmaceutical and medicinal treatments.

The simulation, modeling and docking tools gave a tremendously valuable guide for selecting the most suitable compounds for specific action, where the theoretical view nearby is coincidence with the laboratory results.

## 5. Acknowledgement

The authors are grateful to Professor Adel S. Orabi, Department of Inorganic chemistry, Suez Canal University, Ismailia, Egypt, for his generous support. His sincere aid in facilitating the use of Molecular Docking is highly appreciated.

## References

- [1] V. V Kouznetsov, L.Y. Vargas Méndez, C.M. Meléndez Gómez, Recent Progress in the Synthesis of Quinolines, *Curr. Org. Chem.* 9 (2005) 141–161. doi:10.2174/1385272053369196.
- [2] R. Musiol, J. Jampilek, V. Buchta, L. Silva, H. Niedbala, B. Podeszwa, A. Palka, K. Majerz-Maniecka, B. Oleksyn, J. Polanski, Antifungal properties of new series of quinoline derivatives, *Bioorg. Med. Chem.* 14 (2006) 3592–3598. doi:10.1016/j.bmc.2006.01.016.
- [3] C. Bénard, F. Zouhiri, M. Normand-Bayle, M. Danet, D. Desmaële, H. Leh, J.-F.F. Mouscadet, G. Mbemba, C.M. Thomas, S. Bonnenfant, M. Le Bret, J. D'Angelo, Linker-modified quinoline derivatives targeting HIV-1 integrase: Synthesis and biological activity, *Bioorganic Med. Chem. Lett.* 14 (2004) 2473–2476. doi:10.1016/j.bmcl.2004.03.005.
- [4] J. Desrivot, C. Herrenknecht, G. Ponchel, N. Garbi, E. Prina, A. Fournet, C. Bories, B. Figadère, R. Hocquemiller, P.M. Loiseau, Antileishmanial 2-substituted quinolines: In

- vitro behaviour towards biological components, *Biomed. Pharmacother.* 61 (2007) 441–450. doi:10.1016/j.biopha.2007.03.004.
- [5] A. Borioni, C. Mustazza, I. Sestili, M. Sbraccia, L. Turchetto, M.R. Del Giudice, Synthesis of new 4-heteroaryl-2-phenylquinolines and their pharmacological activity as NK-2/NK-3 receptor ligands, *Arch. Pharm. (Weinheim)*. 340 (2007) 17–25. doi:10.1002/ardp.200600113.
- [6] B.E. Evans, K.E. Rittle, M.G. Bock, R.M. DiPardo, R.M. Freidinger, W.L. Whitter, G.F. Lundell, D.F. Veber, P.S. Anderson, R.S.L. Chang, V.J. Lotti, D.J. Cerino, T.B. Chen, P.J. Kling, K.A. Kunkel, J.P. Springer, J. Hirshfield, Methods for drug discovery: development of potent, selective, orally effective cholecystokinin antagonists, *J. Med. Chem.* 31 (1988) 2235–2246. doi:10.1021/jm00120a002.
- [7] S. Bräse, *Privileged Scaffolds in Medicinal Chemistry: Design, Synthesis, Evaluation*, Royal Society of Chemistry, London, UK, 2015.
- [8] V.R. Solomon, H. Lee, *Quinoline as a Privileged Scaffold in Cancer Drug Discovery*, *Curr. Med. Chem.* 18 (2011) 1488–1508.
- [9] A. Koul, E. Arnoult, N. Lounis, J. Guillemont, K. Andries, The challenge of new drug discovery for tuberculosis, *Nature*. 469 (2011) 483–490. doi:10.1038/nature09657.
- [10] M.C. Mandewale, B. Thorat, Y. Nivid, R. Jadhav, A. Nagarsekar, R. Yamgar, Synthesis, structural studies and antituberculosis evaluation of new hydrazone derivatives of quinoline and their Zn(II) complexes, *J. Saudi Chem. Soc.* 22 (2018) 136–145. doi:10.1016/j.jscs.2016.04.003.
- [11] M. Dinakaran, P. Senthilkumar, P. Yogeewari, A. China, V. Nagaraja, D. Sriram, Antimycobacterial activities of novel 2-(sub)-3-fluoro/nitro-5,12-dihydro-5-oxobenzothiazolo[3,2-a]quinoline-6-carboxylic acid, *Bioorg. Med. Chem.* 16 (2008) 3408–3418. doi:10.1016/j.bmc.2007.11.016.
- [12] A. Lilienkampf, M. Jialin, W. Baojie, W. Yuehong, S.G. Franzblau, A.P. Kozikowski, Structure-Activity relationships for a series of quinoline-based compounds active against replicating and nonreplicating mycobacterium tuberculosis, *J. Med. Chem.* 52 (2009) 2109–2118. doi:10.1021/jm900003c.
- [13] S. Eswaran, A.V. Adhikari, I.H. Chowdhury, N.K. Pal, K.D. Thomas, New quinoline derivatives: Synthesis and investigation of antibacterial and antituberculosis properties, *Eur. J. Med. Chem.* 45 (2010) 3374–3383.

- doi:10.1016/j.ejmech.2010.04.022.
- [14] S. Rollas, Ş.G. Küçükgülzel, Biological activities of hydrazone derivatives, *Molecules*. 12 (2007) 1910–1939. doi:10.3390/12081910.
- [15] E. Vavříková, S. Polanc, M. Kočevár, K. Horváti, S. Bsze, J. Stolaříková, K. Vávrová, J. Vinšová, New fluorine-containing hydrazones active against MDR-tuberculosis, *Eur. J. Med. Chem.* 46 (2011) 4937–4945. doi:10.1016/j.ejmech.2011.07.052.
- [16] K.D. Thomas, A.V. Adhikari, S. Telkar, I.H. Chowdhury, R. Mahmood, N.K. Pal, G. Row, E. Sumesh, Design, synthesis and docking studies of new quinoline-3-carbohydrazide derivatives as antitubercular agents, *Eur. J. Med. Chem.* 46 (2011) 5283–5292. doi:10.1016/j.ejmech.2011.07.033.
- [17] M.C. Mandewale, B.R. Thorat, R.S. Yamgar, Synthesis and anti-mycobacterium study of some fluorine containing schiff bases of quinoline and their metal complexes, *Der Pharma Chem.* 7 (2015) 207–215.
- [18] I. Kostova, S. Balkansky, Metal Complexes of Biologically Active Ligands as Potential Antioxidants, *Curr. Med. Chem.* 20 (2013) 4508–4539.
- [19] E.K. Efthimiadou, G. Psomas, Y. Sanakis, N. Katsaros, A. Karaliota, Metal complexes with the quinolone antibacterial agent N-propyl-norfloxacin: Synthesis, structure and bioactivity, *J. Inorg. Biochem.* 101 (2007) 525–535. doi:10.1016/j.jinorgbio.2006.11.020.
- [20] A.L. Barry, S.D. Brown, Fluconazole disk diffusion procedure for determining susceptibility of *Candida* species . Fluconazole Disk Diffusion Procedure for Determining Susceptibility of *Candida* Species, *J. Clin. Microbiol.* 34 (1996) 2154–2157.
- [21] R. Cruickshank, J.P. Duguid, R.H.A. Swain, *The Practice of medical microbiology*, 11th ed., E&S Livingstone Ltd, Edinburgh □ London, UK, 1965.
- [22] A.S. Orabi, K.M. Abou El-Nour, M.F. Youssef, H.A. Salem, Novel and highly effective composites of silver and zinc oxide nanoparticles with some transition metal complexes against different microorganisms, *Arab. J. Chem.* (2018). doi:10.1016/J.ARABJC.2018.06.016.
- [23] P. Tyagi, S. Chandra, B.S. Saraswat, D. Yadav, Design, spectral characterization, thermal, DFT studies and anticancer cell line activities of Co(II), Ni(II) and Cu(II)

- complexes of Schiff bases derived from 4-amino-5-(pyridin-4-yl)-4H-1,2,4-triazole-3-thiol, *Spectrochim. Acta - Part A Mol. Biomol. Spectrosc.* 145 (2015) 155–164. doi:10.1016/j.saa.2015.03.034.
- [24] A.S. Orabi, F.S. Deghaidy, H. a. Azab, H. Said, Physico-Chemical Properties of Nd(III) and Er(III) Complexes With Some Biological Buffer Ligands, *Synth. React. Inorg. Met. Chem.* 31 (2001) 695–711. doi:10.1081/SIM-100104797.
- [25] A.S. Orabi, Complexes derived from some biologically active ligands, *J. Coord. Chem.* 61 (2008) 1294–1305. doi:10.1080/00958970701573160.
- [26] Q. Wang, Y. Pan<sup>1</sup>, J. Wang, Q. Peng, H. Luo, J. Zheng<sup>1</sup>, Synthesis and biological activities of substituted N'-benzoylhydrazone derivatives, *African J. Biotechnol.* 10 (2011) 18013–18021. doi:10.5897/AJB10.2501.
- [27] N.L. Alpert, W.E. Keiser, H.A. Szymanski, *Theory and Practice of Infrared Spectroscopy*, 2nd ed., Plenum Press, New York, USA, 1970.
- [28] K. Nakamoto, *Infrared and Raman Spectra of Inorganic and Coordination Compounds, Part II: Application in Coordination, Organometallic, and Bioinorganic Chemistry*, 5th ed., Wiley, New York, 1997.
- [29] A.S. Orabi, A.M. Abbas, S.A. Sallam, Spectral, magnetic, thermal, and DNA interaction of Ni(II) complexes of glutamic acid schiff bases, *Synth. React. Inorganic, Met. Nano-Metal Chem.* 43 (2013) 63–75. doi:10.1080/15533174.2012.684260.
- [30] D.L. Pavia, G.M. Lampman, G.S. Kriz, *Introduction to Spectroscopy*, 2nd ed., Saunders Golden Sunburst Series, 1997.
- [31] E. Cazedey, H. Salgado, Spectrophotometric Determination of Ciprofloxacin Hydrochloride in Ophthalmic Solution, *Adv. Anal. Chem.* 2 (2012) 74–79. doi:10.5923/j.aac.20120206.01.
- [32] J.W. Robinson, E.M.S. Frame, G.M. Frame, *Undergraduate Instrumental Analysis, Seventh*, CRC Press Taylor & Francis Group, New York, NY, 2014.
- [33] M.L. Dianu, A. Kriza, A.M. Musuc, Synthesis, spectral characterization, and thermal behavior of mononuclear Cu(II), Co(II), Ni(II), Mn(II), and Zn(II) complexes with 5-bromosalicylaldehyde isonicotinoylhydrazone, *J. Therm. Anal. Calorim.* 112 (2013) 585–593. doi:10.1007/s10973-012-2578-x.
- [34] V.P. Singh, S. Singh, D.P. Singh, K. Tiwari, M. Mishra, Synthesis, spectroscopic

- (electronic, IR, NMR and ESR) and theoretical studies of transition metal complexes with some unsymmetrical Schiff bases, *J. Mol. Struct.* 1058 (2014) 71–78. doi:10.1016/j.molstruc.2013.10.046.
- [35] B.N. Figgis, J. Lewis, J. Lewis, R.G. Wilkins, *Magnetochemistry of Complex Compounds in Modern Coordination Chemistry*, Interscience, New York, 1960.
- [36] T.G. Dunne, Magnetic moment measurement of a coordination complex: An experiment in undergraduate inorganic chemistry, *J. Chem. Educ.* 44 (1967) 142–144. doi:10.1021/ed044p142.
- [37] Z.S. Teweldemedhin, R.L. Fuller, M. Greenblatt, Magnetic Susceptibility Measurements of Solid Manganese Compounds with Evan's Balance, *J. Chem. Educ.* 73 (1996) 906–909. doi:10.1021/ed073p906.
- [38] M.A. Mahmoud, S.A. Zaitone, A.M. Ammar, S.A. Sallam, Synthesis, spectral, thermal and insulin-enhancing properties of oxovanadium(IV) complexes of metformin Schiff-bases, *J. Therm. Anal. Calorim.* 128 (2017) 957–969. doi:10.1007/s10973-016-6018-1.
- [39] H.M. Aly, M.E. Moustafa, M.Y. Nassar, E.A. Abdelrahman, Synthesis and characterization of novel Cu (II) complexes with 3-substituted-4-amino-5-mercapto-1,2,4-triazole Schiff bases: A new route to CuO nanoparticles, *J. Mol. Struct.* 1086 (2015) 223–231. doi:10.1016/j.molstruc.2015.01.017.
- [40] H.F. Abd El-Halim, G.G. Mohamed, E.A.M. Khalil, Synthesis, spectral, thermal and biological studies of mixed ligand complexes with newly prepared Schiff base and 1,10-phenanthroline ligands, *J. Mol. Struct.* 1146 (2017) 153–163. doi:10.1016/j.molstruc.2017.05.092.
- [41] Adel S. Orabi, H.K. Ibrahim, E.-S.H. EL-Tamany, A. Radwan, Studies of Some New Biologically Active Ligands and Their Complexes Derived from Some Transition Metal Ions, *Asian J. Chem.* 20 (2008) 2022–2036. <http://www.tandfonline.com/doi/abs/10.1080/00958970701573160>.
- [42] Zia-ur-Rehman, A. Shah, K.S. Munawar, A.A. Khan, R. Abbasi, M.A. Yameen, A.M. Khan, A.R. Khan, I.Z. Qureshi, H.B. Kraatz, Synthesis, spectroscopic characterization, DFT optimization and biological activities of Schiff bases and their metal (II) complexes, *J. Mol. Struct.* 1145 (2017) 132–140. doi:10.1016/j.molstruc.2017.05.098.
- [43] Xavier.T.S, I.H. Joe, FT-IR, Raman and DFT study of 2-amino-5-fluorobenzoic acid and its biological activity with other halogen (Cl, Br) substitution, *Spectrochim. Acta*

- Part A Mol. Biomol. Spectrosc. 79 (2011) 332–337. doi:10.1016/j.saa.2011.02.037.
- [44] P. Tyagi, M. Tyagi, S. Agrawal, S. Chandra, H. Ojha, M. Pathak, Synthesis, characterization of 1,2,4-triazole Schiff base derived 3d-metal complexes: Induces cytotoxicity in HepG2, MCF-7 cell line, BSA binding fluorescence and DFT study, Spectrochim. Acta - Part A Mol. Biomol. Spectrosc. 171 (2017) 246–257. doi:10.1016/j.saa.2016.08.008.
- [45] G.L. Patrick, An Introduction to Medicinal Chemistry, 5th ed., Oxford University Press, Oxford, United Kingdom, 2013. doi:10.1017/CBO9781107415324.004.

- New complexes with new promising properties.
- The most stable structure was obtained *In silico* level.
- The antimicrobial activity *in vitro* level gave very promising results
- The Docking work with HepG2 gave the bonding site and its energy
- Novel Cu(II) complexes gave very promising antimicrobial activity

ACCEPTED MANUSCRIPT